UCL Université catholique de Louvain

École polytechnique de Louvain (EPL)

epl

Influence of the relaxation time approximation on first principle study of transport coefficients in thermoelectric material PbTe

Dissertation presented by
Jean-Baptiste VAN DEN EYNDE

for obtaining the Master's degree in
Physical Engineering

Supervisor(s)
Geoffroy HAUTIER , Gian-Marco RIGNANESE

Reader(s)
Jean-Christophe CHARLIER, Pascal JACQUES

Academic year 2015-2016

Acknowledgments

I would like to express my very great appreciation to all those who provided me the possibility to complete this report. I give a special thanks to my supervisors, Prof. Geoffroy Hautier and Prof. Gian-Marco Rignanese, whose contribution in useful suggestions, advices and encouragement, helped me to coordinate my project especially in writing this report.

Furthermore I also wish to acknowledge with much appreciation the valuable assistance provided by Dr. Francesco Ricci for the utilization and understanding of the BoltzTraP program.

My grateful thanks are also extended to Mr. Yannick Gillet for his patient help with the Abinit program and to Mr. Guillaume Brunin and Mr. Grégoire Thunis for the stimulating discussions and suggestions.

Finally, I would like to thank my parents for their support and encouragements throughout my studies.

The computing resources were provided by *Centre de calcul intensif et de stockage de masse* (CISM) of the *Université Catholique de Louvain* partner of the *Consortium des Equipement de Calcul Intensif* (CECI) of the federation Wallonia-Brussels.

Contents

Chapter 1

Introduction

Since a few decades, the environmental impact of global climate change has become increasingly alarming and the human responsibility of this change through the combustion of fossil fuels is now clearly established. Moreover the world energy consumption is growing every year. It has thus become essential to improve the energy efficiency in order to reduce our dependence on fossil fuels. One possible solution for obtaining a more sustainable energy base is the recovery of wasted heat. Thermoelectric materials are of great interest in this framework since they can convert directly temperature differences into electric voltage (and vice versa) and can thus be used to harvest waste heat energy. Although the efficiency of thermoelectric generators is rather low, typically 5% [1], the other advantages, such as compactness, silent, reliability, long life, and long period of operation without attention, led to a wide range of applications. Lead telluride (PbTe) thermoelectric generators have been widely used by the US army, in space crafts to provide on-board power, and in pacemakers batteries [2] but until now the low efficiency kept them away from commercial use. Recent researches in thermoelectricity aim to obtain new improved materials for heat waste recovery, such as the conversion of auto-mobile or power plant exhaust heat into electricity.

In this master thesis, we have performed an ab-initio study of transport properties in thermoelectric materials and in particular lead telluride. Ab-initio methods are simulation techniques in which the quantum equations governing the electronic behaviour in a crystal are solved without any adjustable parameter. First-principle simulations make it possible to predict the properties of materials even before synthesizing them and are very useful in understanding the quantum world without effectively testing a material in the laboratory. Obviously, in the search for more efficient thermoelectric materials, quantum simulation is an essential tool that will play a significant role. The transport properties of PbTe have been simulated by the use of two open-source programs : ABINIT [3] and BOLTZTRAP [4]. ABINIT implements the *Density Functional Theory* (DFT) by solving the Kohn–Sham equations describing the electrons in a material. We have used it for computing the electronic band structure of lead telluride. The latter has then been used in BOLTZTRAP to compute the transport coefficients by solving the semi-classical *Boltzmann Transport Equation* (BTE) in the *Relaxation Time Approximation* (RTA).

Lead telluride is a well known narrow band gap semiconductor that is widely used as a thermoelectric material, it has been already actively studied and experimental data's are easily available in the literature. The aim of this work is to study the influence of the *Relaxation Time Approximation* when solving the *Boltzmann Transport Equation*. Different models have been tested, from a very simple constant relaxation time to more sophisticated models including energy and temperature dependence determined by the nature of scattering. For each model, the transport coefficients have been computed and compared to experimental data in order to check their accuracy.

The present thesis is organised as follows. Chapter 2 describes the thermoelectric effect and how it can be used to generate electrical power. Chapter 3 describes the general properties of lead

telluride, the structural relaxation of its unit cell and its computed band structure. Chapter 4 presents the semi-classical Boltzmann transport theory, starting from the derivation of the Boltzmann equation and followed by the introduction of the *Relaxation Time Approximation*, the computation of transport coefficients in this theory and the working principle of the BoltzTraP program. In Chapter 5 the dominant scattering mechanisms present in PbTe are explained along with the different models for the relaxation time. Our implementation of these models in BoltzTraP is also described. Chapter 6 presents the transport coefficients of PbTe obtained with the different relaxation times derived in the previous chapter and compares them to the experimental results. Finally Chapter 7 summarizes the main results of this work and how it could be continued.

Chapter 2

Thermoelectricity

Contents

This section was inspired by Refs. [5], [6] and [7].

The thermoelectric effect is the direct conversion of temperature differences to electric voltage and vice versa. A thermoelectric device creates a voltage when there is a different temperature on each side of it. Conversely, when a voltage is applied to the device, it creates a temperature difference. At the atomic scale, an applied temperature gradient causes charge carriers in the material to diffuse from the hot side to the cold side.

This effect can be used to generate electricity (see below), measure temperature or change the temperature of objects. Because the direction of heating and cooling is determined by the polarity of the applied voltage, thermoelectric devices can be used as temperature controllers.

The term "thermoelectric effect" encompasses three separately identified effects: the Seebeck effect, Peltier effect, and Thomson effect.

2.1 Seebeck Effect

At the atomic scale, the Seebeck effect can be attributed to two contributions : charge carriers diffusion and phonon-drag. First when a temperature gradient is applied to a material, it causes charge carriers to diffuse from the hot side to the cold side and this contributes to the creation of a thermoelectric field called the Seebeck field. Secondly the phonons in the material are not in thermal equilibrium due to the temperature gradient and they tend to travel against it. As they move, they interact with electrons by transferring momentum and electrons are then pushed towards the cold side of the material. This phenomenon called phonon-drag reinforce the already existing thermoelectric field [8].

The Seebeck effect is a classical example of an electromotive force (emf) and leads to measurable currents or voltages in the same way as any other emf. Electromotive forces modify Ohm's law by generating currents even in the absence of voltage differences (or vice versa); the local current density $\boldsymbol{J}$ is given by

$$\boldsymbol{J} = \sigma(-\boldsymbol{\nabla} V + \boldsymbol{E}_{emf}) \tag{2.1}$$

where V is the local voltage and σ is the local conductivity. In general, the Seebeck effect is described locally by the creation of an electromotive field

$$E_{emf} = -S\boldsymbol{\nabla}T \tag{2.2}$$

where S is the Seebeck coefficient (also known as thermopower), a local property of the material, and $\boldsymbol{\nabla}T$ is the gradient in temperature T.

The Seebeck coefficient is measured in $\mathrm{V\,K^{-1}}$ or more generally $\mu\mathrm{V\,K^{-1}}$. It generally varies as function of temperature, and depends strongly on the composition of the conductor. If the system reaches a steady state where $\boldsymbol{J} = 0$, then the voltage gradient is given simply by the electromotive force :

$$-\boldsymbol{\nabla}V = S\boldsymbol{\nabla}T \tag{2.3}$$

2.2 Peltier Effect

The Peltier effect is the presence of heating or cooling at an electrified junction of two different conductors. When a current is made to flow through a junction between two conductors A and B, heat may be generated (or removed) at the junction. The Peltier heat generated at the junction per unit time, $\dot{Q}$, is equal to

$$\dot{Q} = (\Pi_{\mathrm{A}} - \Pi_{\mathrm{B}})\, I \tag{2.4}$$

where Π_{A} (Π_{B}) is the Peltier coefficient of conductor A (B), and I is the electric current (from A to B). The total heat generated is not determined by the Peltier effect alone, as it may also be influenced by Joule heating and thermal gradient effects.

The Peltier coefficient represents how much heat is carried per charge unit. Since charge current must be continuous across a junction, the associated heat flow will develop a discontinuity if Π_{A} and Π_{B} are different. The Peltier effect can be considered as the back-action counterpart of the Seebeck effect: if a simple thermoelectric circuit is closed then the Seebeck effect will drive a current, which in turn (via the Peltier effect) will always transfer heat from the hot to the cold junction.

2.3 Thomson Effect

In many materials, the Seebeck coefficient is not constant in temperature, and so a spatial gradient in temperature can result in a gradient in the Seebeck coefficient. If a current is driven through this gradient then a continuous version of the Peltier effect will occur. The Thomson effect describes the heating or cooling of a current-carrying conductor with a temperature gradient.

If a current density $\boldsymbol{J}$ is passed through a homogeneous conductor, the Thomson effect predicts a heat production rate $\dot{q}$ per unit volume of:

$$\dot{q} = -\mathcal{K}\boldsymbol{J}\cdot\boldsymbol{\nabla}T \tag{2.5}$$

where $\mathcal{K}$ is the Thomson coefficient.

2.4 Thomson Relations

There exist relationships between the three thermoelectric coefficients called the Thomson relations. The first relation is

$$\mathcal{K} \equiv \frac{d\Pi}{dT} - S \tag{2.6}$$

This relationship is easily shown given that the Thomson effect is a continuous version of the Peltier effect. The second Thomson relation is

$$\Pi = TS \tag{2.7}$$

Using Eq. (2.7), the first Thomson relation becomes

$$\mathcal{K} = T\frac{dS}{dT}. \tag{2.8}$$

This equation however neglects Joule heating, and ordinary thermal conductivity.

The Thomson relations imply that these three effects are different manifestations of only one thermoelectric effect. Therefore only one coefficient is needed to fully describe the thermoelectric properties of a material, and the Seebeck coefficient S was chosen.

2.5 Power Generation

As seen before, the thermoelectric effect can be used to produce energy in presence of a temperature gradient. Thermoelectric generators (TEGs) are made of thermocouples consisting of two dissimilar thermoelectric materials joining in their ends: an n-type (negatively charged) and a p-type (positively charged) semiconductors. When there is a temperature difference, charge carriers will diffuse from the hot side to the cold side of the module. Since the charge carriers are electrons in the n-type material and electron holes in the p-type material, their diffusion will generate a direct electric current in the circuit (see Figure 2.1). A thermocouple produces low voltage and high current. Thus, to obtain high voltages, TEGs are made of several thermocouples connected electrically in series and thermally in parallel.

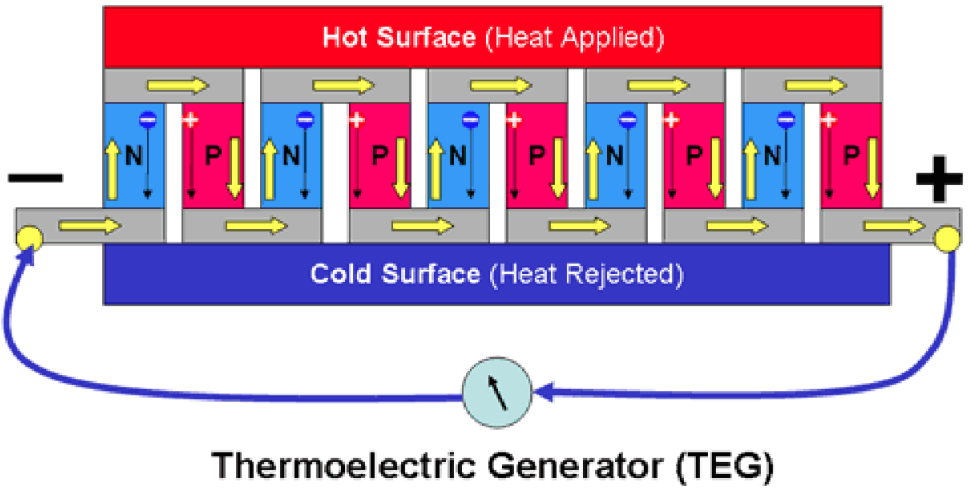

Figure 2.1: A thermoelectric circuit composed of materials of different Seebeck coefficient (p-doped and n-doped semiconductors), assembled in modules configured as a thermoelectric generator (reproduced from Woodbank Communications Ltd [9]).

Thermoelectric generators (TEGs) function like heat engines, but are less bulky and have no moving parts. However, TEGs are typically more expensive and less efficient and serve then application niches where efficiency and cost are less important than reliability, light weight, and small size.

Thermoelectric generators could be used in power plants in order to convert waste heat into additional electrical power and in automobiles as automotive thermoelectric generators to

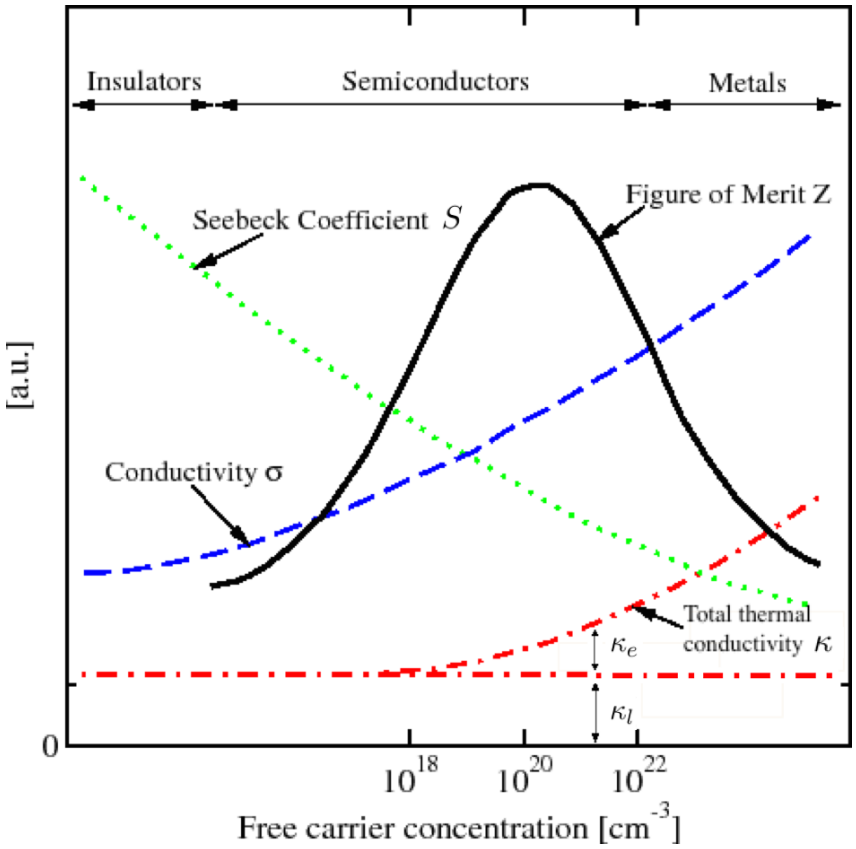

Figure 2.2: Dependence of Seebeck coefficient S, electrical conductivity σ and thermal conductivity κ (κ_e and κ_l) on the concentration of free carriers. (Adapted from M. Wagner [10]).

increase fuel efficiency. They are already employed in radioisotope thermoelectric generators which are used in space probes and have the same mechanism but use radioisotopes to generate the required heat difference.

2.6 Thermoelectric Materials

In order to maximize the TEGs efficiency, the use of good thermoelectric materials is essential. Good thermoelectric materials must have a high electrical conductivity σ, to facilitate carrier diffusion from hot side to cold side, a low thermal conductivity κ ($= \kappa_e + \kappa_l$) and a high Seebeck coefficient. A low thermal conductivity ensures that when one side is made hot, the other side stays cold, which helps to generate a large voltage. These requirements are summarized in what is called the *Figure of merit* (FOM) zT:

$$zT = \frac{\sigma S^2 T}{\kappa_e + \kappa_l} \tag{2.9}$$

Figure 2.2 shows the dependence of the three parameters appearing in the figure of merit on the carrier concentration. From this figure, it is seen that the FOM reaches its maximum value around a carrier concentration of 10^{20}cm^{-3} [1], which corresponds to heavily doped or near degenerate semiconductors. The precise carrier concentration to maximize zT depends on temperature and on the specific semiconductor.

From the definition of the figure of merit (Eq. (2.9)), it is clear that in order to improve the efficiency of a thermoelectric material, the thermal conductivity must be decreased and the numerator of z: σS^2 known as power factor (PF) has to be increased.

Since the electronic thermal conductivity is related to electric conductivity by the Wiedemann-Franz law [11] :

$$\frac{\kappa_e}{\sigma T} = L_0 = \frac{\pi^2}{3}\left(\frac{k_B}{e}\right)^2 = 2.44 \cdot 10^{-8}\ \mathrm{W\,\Omega\,K^{-2}}, \tag{2.10}$$

increasing σ leads to increase κ_e. Therefore reducing the total thermal conductivity is achieved by acting on the lattice thermal conductivity κ_l. Today κ_l of semiconductors can be lowered without affecting their high electrical properties using nanotechnology. This can be made by creating nano-scale features such as particles, wires or interfaces in bulk semiconductor materials. However, the manufacturing processes of nano-materials is still challenging and very expensive.

The other way to raise the FOM is to boost the power factor σS^2 by varying the doping concentration and manipulating the electronic structure in the neighbourhood of the chemical potential. Most thermoelectric materials today have a zT value around unity, such as Bismuth Telluride (Bi_2Te_3) at room temperature and lead telluride at 500-700 K.

The thermoelectric materials that are employed in commercial applications such as TEGs can be divided into three groups based on the temperature range of operation [7]:

1. Low temperature materials (up to around 450K): Alloys based on Bismuth (Bi) in combinations with Antimony (Sb), Tellurium (Te) or Selenium (Se).

2. Intermediate temperature (up to 850K): such as materials based on alloys of Lead (Pb)

3. Highest temperature materials (up to 1300K): materials fabricated from silicon germanium (SiGe) alloys.

Although these materials still remain the base for commercial and practical applications in thermoelectric power generation, significant advances have been made in synthesizing new materials and fabricating material structures with improved thermoelectric performance [12] [13].

Chapter 3

Lead Telluride

Contents

3.1 General Properties

Lead telluride is a narrow gap semiconductor considered as an intermediate thermoelectric material. Its operating temperature range is between 300 and 900 K. PbTe has a high melting point, good chemical stability, low vapor pressure and good chemical strength in addition to high figure of merit (~ 1).

3.1.1 Crystal Structure

PbTe crystallizes in the NaCl crystal structure, i.e. a rocksalt structure corresponding to a face-centered cubic system (FCC) with Te atoms forming the anionic lattice and Pb atoms occupying the octahedral cation sites. Alternately, one could view this structure as two separate face-centered cubic lattices formed by Pb and Te atoms, with the two lattices interpenetrating. Figure 3.1 represents the cubic unit cell. The space group of the rock-salt structure is called $Fm\bar{3}m$ in Hermann–Mauguin notation. The coordination number of each atom in this structure is 6: each cation is coordinated to 6 anions at the vertices of an octahedron, and similarly, each anion is coordinated to 6 cations at the vertices of an octahedron.

The cubic unit cell shown in Figure 3.1 is not the simplest repeating unit of the structure and is then not the primitive unit cell. Lead telluride has a trigonal primitive cell with a unique lattice parameter: $a = b = c$ and a unique cell angle: $\alpha = \beta = \gamma = 60°$ (see Figure 3.2). This unit cell contains two atoms : one Te atom at position [0 0 0] and one Pb atom at position [0.5 0.5 0.5]. A structural relaxation will be realised in the next section to calculate precisely the lattice parameter a.

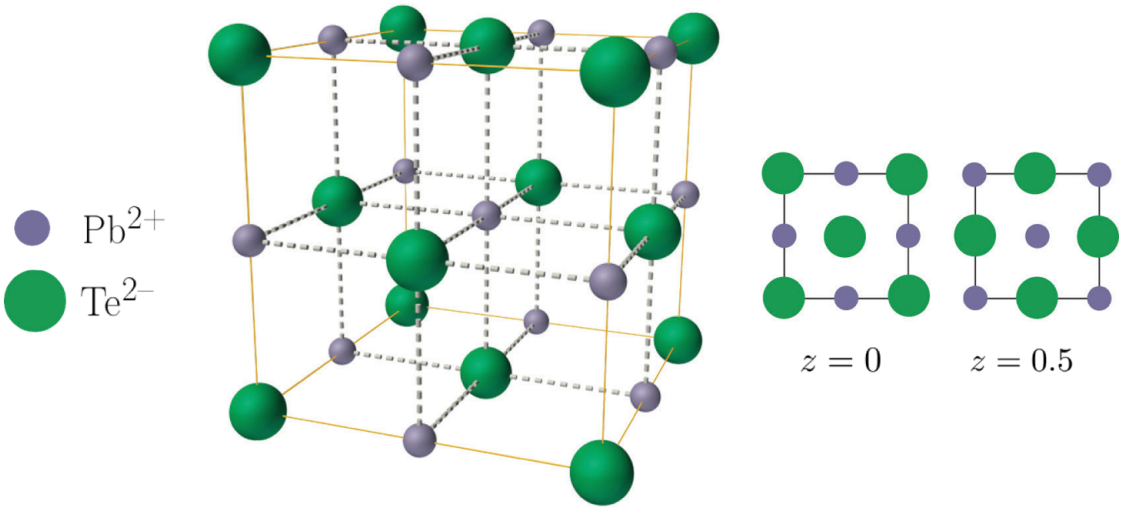

Figure 3.1: Left: Cubic cell structure of lead telluride. Right: Top view of the structure in the plans $z = 0$ and $z = 0.5$. (Adapted from UC Davis ChemWiki [14]).

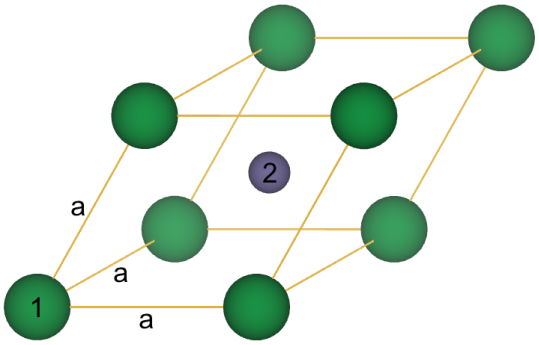

Figure 3.2: Trigonal primitive cell structure used in calculations. The cell contains two atoms, one Te atom at reduced coordinates [0 0 0] labelled as 1 and one Pb atom at reduced coordinates [0.5 0.5 0.5] labelled as 2. (Drawn with Vesta [15]).

3.1.2 Doping

As seen in the previous section, the thermoelectric materials with the highest figure of merit correspond to highly doped semiconductors. Doping a semiconductor in a crystal introduces allowed energy states in the band gap. The new gap between these energy states and the nearest energy band is usually small, so that room temperature is hot enough to thermally ionize practically all of the dopant atoms and create free charge carriers in the conduction or valence bands. PbTe can be a n- or p-type material as a result of deviation from stoichiometry, (Pb-rich PbTe is n-type, while Te-rich PbTe is p-type). The electrical properties of PbTe are greatly affected by adding foreign atoms to the PbTe lattice. The possible doping agents are discussed in Ref. [1] and summarized as follows; halogen atoms may be used via $PbCl_2$, $PbBr_2$ or PbI_2 to produce donor centers. Other n-type doping agents such as Bi_2Te_3, $TaTe_2$, $MnTe_2$, can be added to PbTe, they substitute for Pb and thus create uncharged Pb vacancies. These vacant sites are subsequently filled by atoms from the lead excess. Because the valence electrons of these vacancies are not involved in a chemical bond, they diffuse through the crystal. Alkali acceptor agents may be used to produce p-type PbTe. Doping agents such as Na_2Te, K_2Te, Ag_2Te substitute for Te and create uncharged Te vacancies. These sites are filled by Te atoms which are ionized to create additional positive holes. The free electron (n-type) or hole concentration (p-type) in PbTe is the sum of the electrons or holes originating from Pb or Te in solution plus

the electrons or holes introduced by the donor or acceptor species.

3.1.3 Spin-orbit Coupling

In quantum physics, the spin–orbit coupling (SOC) is a relativistic interaction of a particle's spin with its motion. It may lead to the lifting of degeneracy of one-electron energy levels in atoms, molecules, and solids leading to a modified band structure. This splitting occurs due to electromagnetic interaction between the electron's spin and the magnetic field generated by the electron's orbit around the nucleus. This effect is relativistic and can be fully described by the Dirac equation [16]

$$i\hbar\frac{\partial\psi}{\partial t}(\mathbf{r},t) = \left(\alpha_0 m_0 c^2 - i\hbar c\sum_{j=1}^{3}\alpha_j\frac{\partial}{\partial r_j}\right)\psi(\mathbf{r},t) \tag{3.1}$$

where $\psi(\mathbf{r},t)$ is a four components wave function and α_j, $j = 0,1,2,3$ are 4×4 dimensions matrices acting on ψ and called Dirac matrices.

However in electron band-structure calculations, the non-relativistic Schrödinger equation is frequently used as a first approximation. Without relativistic corrections, it leads to doubly-degenerated bands, spin-up and spin-down, which can be split by a spin-dependent term in the Hamiltonian. In this approach, spin-orbit interaction can be included as a relativistic correction to the Schrödinger equation instead of using the Dirac equation. This is the approach implemented in the ABINIT program used in this work for the band structure calculation.

The spin-orbit coupling for a single atom (hydrogen like atoms) can be illustrated in the framework of the classical electrodynamics, where the vectors of the electromagnetic field depend on the reference system. Although in the rest frame of the nucleus, there is no magnetic field acting on the electron, there is one in the rest frame of the electron. In a reference system that moves with velocity $\boldsymbol{v}$ relative to a radial electric field $\boldsymbol{E} = |E/r|\boldsymbol{r}$, one finds a magnetic field [17]

$$\boldsymbol{B} = -\frac{1}{c^2}\boldsymbol{v}\times\boldsymbol{E} = \frac{1}{m_0 c^2}\left|\frac{E}{r}\right|(\boldsymbol{r}\times\boldsymbol{p}) \tag{3.2}$$

where terms of order $(v/c)^2$ and higher order terms are neglected. In the case of centrally symmetric electrical fields, as e.g. the orbital motion of an electron in the electric field of an atomic nucleus, the electric field can be expressed as the gradient of the electric potential $\boldsymbol{E} = -\boldsymbol{\nabla}V_{el}$

$$|E| = \frac{\partial V_{el}}{\partial r} = \frac{1}{e}\frac{\partial V}{\partial r} \tag{3.3}$$

where $V = eV_{el}$ is the potential energy of the electron in the central field. From classical mechanics, the angular momentum $\boldsymbol{l}$ of a particle is equal to $\boldsymbol{l} = \boldsymbol{r}\times\boldsymbol{p}$. Injecting this and Eq. (3.3) into Eq. (3.2) leads to

$$\boldsymbol{B} = \frac{1}{m_0 c^2 e}\frac{1}{r}\frac{\partial V}{\partial r}\boldsymbol{l} \tag{3.4}$$

The spin magnetic moment of the electron is

$$\boldsymbol{\mu_s} = -g_S\mu_B\frac{\mathbf{s}}{\hbar} \tag{3.5}$$

where $\boldsymbol{s}$ is the spin angular momentum vector, μ_B is the Bohr magneton ($\mu_B = \frac{e\hbar}{2m_0}$) and $g_\mathrm{s} \approx 2$ is the electron spin Lande factor (or g-factor). Classically it should be 1, but it is 2 according to Dirac's relativistic quantum theory. Putting all together we obtain

$$\boldsymbol{\mu_s} = -\frac{e}{m_0}\boldsymbol{s} \tag{3.6}$$

The interaction of the magnetic moment of the electron with the magnetic field of the nucleus in the co-moving frame of the electron is called the Larmor interaction energy and is given by

$$\Delta H_\mathrm{L} = -\boldsymbol{\mu_s}\cdot\boldsymbol{B}. \tag{3.7}$$

Substituting in this equation expressions for the magnetic moment and the magnetic field, one gets

$$\Delta H_{\mathrm{L}} = \frac{1}{m_0^2 c^2} \frac{1}{r} \frac{\partial V}{\partial r} (\boldsymbol{l} \cdot \boldsymbol{s}) \tag{3.8}$$

The spin-orbit energy shift is obtained by multiplying the Larmor energy by a factor 1/2 called Thomas factor coming from the Thomas precession correction for the electron's curved trajectory corresponding to an non-inertial frame [17].

$$\Delta H_{\mathrm{SO}} = \frac{1}{2m_0^2 c^2} \frac{1}{r} \frac{\partial V}{\partial r} (\boldsymbol{l} \cdot \boldsymbol{s}) \tag{3.9}$$

In solids, spherical symmetry is not present and the contribution of the spin-orbit effect to the Hamiltonian is

$$\Delta H_{\mathrm{SO}} = \frac{1}{2m_0^2 c^2} \boldsymbol{s} \cdot (\boldsymbol{\nabla} V \times \boldsymbol{p}) \tag{3.10}$$

Spin-orbit coupling can then split a spin degenerate level into levels with spin parallel and antiparallel to the orbit. In a free atom, spin-orbit interaction can lift the degeneracy of states with the same orbital (spatial) wave function but with opposite spins. In solids, however, such a splitting can sometimes be forbidden due to crystal symmetry. As a fundamental principle of quantum mechanics, time reversal symmetry always preserves the Kramer's degeneracy between a function $\psi(\boldsymbol{r}, \boldsymbol{s})$ and its complex conjugate $\psi^*(\boldsymbol{r}, \boldsymbol{s})$ [16]. The latter function differs from ψ through a simultaneous reversal of wave vector and electron spin. Therefore, at any point of the Brillouin zone, one can write for the energy

$$\varepsilon(\boldsymbol{k}, \uparrow) = \varepsilon(-\boldsymbol{k}, \downarrow) \tag{3.11}$$

The Kramer's degeneracy remains unaffected when including the spin-orbit interaction term in the Hamiltonian.

If the crystal lattice has inversion symmetry (i.e. if the operation $\boldsymbol{r} \to -\boldsymbol{r}$ does not change the crystal lattice), one will obtain

$$\varepsilon(\boldsymbol{k}, \uparrow) = \varepsilon(-\boldsymbol{k}, \uparrow) \quad \text{and} \quad \varepsilon(\boldsymbol{k}, \downarrow) = \varepsilon(-\boldsymbol{k}, \downarrow) \tag{3.12}$$

From combination of the Eqs. (3.11) and (3.12) it becomes clear that if both time reversal symmetry and inversion symmetry are present, the band structure should satisfy to the condition

$$\varepsilon(\boldsymbol{k}, \uparrow) = \varepsilon(\boldsymbol{k}, \downarrow) \tag{3.13}$$

In other words, the energy cannot depend on the electron spin. Consequently, for crystals which have inversion symmetry like lead telluride, spin splitting is not allowed in the bulk, and these solids keep their spin degeneracy. To conclude in solids there exist two types of spin-orbit interactions : a symmetry-independent and a symmetry-dependent effect. The first one is present in all types of crystals and its importance varies with the considered system but the second one occurs only in non-centrosymmetric crystals. As a consequence in our symmetric system, the SOC will not affect the spin degeneracy in the band structure but it will lift the degeneracy of bands at certain symmetry points of the Brillouin zone (see below).

3.1.4 Pseudopotentials

An introductory description of the *Density Functional Theory* (DFT) can be found in appendix A. In our work, we used the DFT with a plane-wave basis set within the pseudopotential approximation: the "all-electron" atomic potentials are replaced by simpler effective potentials that differ from real ones by the following approximations. First the *frozen core approximation* consists in considering that core electrons are not affected by the environment in which the atom

is placed, the corresponding wavefunctions are considered to be the same as for the isolated atom. This allows one to calculate the wave functions only for valence electrons. Furthermore, the resulting potential (due to the nucleus and core electrons) is replaced by a softer potential (in order to lower the number of plane waves needed to solve the equations) which leads to eigenvalues as close as possible to the original ones. The electronic structures of lead and tellurium are :

$$\mathrm{Pb} : [\mathrm{Xe}]4\mathrm{f}^{14}5\mathrm{d}^{10}6\mathrm{s}^{2}6\mathrm{p}^{2} \tag{3.14}$$

$$\mathrm{Te} : [\mathrm{Kr}]4\mathrm{d}^{10}5\mathrm{s}^{2}5\mathrm{p}^{4} \tag{3.15}$$

Therefore pseudopotentials with 4 valence electrons per lead atom and 6 valence electrons per tellurium atom will be used to compute the electronic properties of lead telluride.

The DFT also include the choice of an approximation for the exchange-correlation potential (see Appendix A for more details). In the case of the pseudopotential approximation explained above, this choice will take place in the selection of the pseudopotentials since they are generated according to the chosen exchange-correlation potential approximation. In this work the *Local density approximation* or LDA is chosen for reasons explained below. The LDA is based on the uniform electrons gas model and is the simplest approach to approximate the exchange-correlation term. It is described as

$$E_{xc}[n] = \int n(\boldsymbol{r})\varepsilon_{xc}[n]dr \tag{3.16}$$

where $\varepsilon_{xc}[n]$ is the exchange-correlation energy of one particle in an homogeneous electron gas and $n(\boldsymbol{r})$ is the electronic density of the first state. The function $\varepsilon_{xc}[n]$ can be decomposed in an exchange part $\varepsilon_x[n]$ and a correlation part $\varepsilon_c[n]$.

$$\varepsilon_{xc}[n] = \varepsilon_x[n] + \varepsilon_c[n] \tag{3.17}$$

The exchange contribution can be calculated analytically :

$$\varepsilon_x[n(r)] = -\frac{3}{4\pi}(3\pi^2 n(r))^{1/3} \tag{3.18}$$

The correlation contribution is obtained from precise numerical simulation (Quantum Monte Carlo).

Since, as mentioned before, spin-orbit coupling is present in PbTe, it is important to choose pseudopentials able to take it into account in the calculations. LDA HGH (Hartwigsen-Goedcker-Hutter) pseudopotentials [18] are good candidates for this since they are fully relativistic norm-conserving pseudopotenials. The used pseudopentials can be found on the ABINIT website [3]

3.2 Convergence Studies and Structural Relaxation

As mentioned before, the calculations are performed in the framework of the density functional theory by the use of the ABINIT program. First of all, this program uses plane waves as basis functions for the calculations. In order to lower the calculation time, only a limited number of plane waves are used, determined by the cut-off energy corresponding to the variable `ecut` in the program. Every vector whose kinetic energy is inferior to `ecut` is used in the plane base. This is possible because the coefficients corresponding to higher energy vectors are smaller in the plane waves base and then of less importance. In consequence, a high `ecut` leads to a great precision but also to a long computation time.

Secondly, the electronic properties depend of the momentum and need then an integration over the Brillouin zone. This is realised by discretizing it in a finite number of k-points [19]. This discretization is controlled by the variable `ngkpt` determining the size of the k-points grid. Again, the more k-points used, the better the precision but the longer the time needed.

In practice a balance between precision and computation time must be found, and it is then important to fix these parameters wisely. This is done through convergence studies of some material properties with a chosen tolerance criteria. The smaller `ecut` and `ngkpt` values leading to converged results according to the tolerance criteria are then used in further calculations.

In this work the assumption that there is no crossed influence of these parameters was made. It means that the convergence in `ecut` is independent from the convergence in `ngkpt`. It is then sufficient to fix one of the parameters to a reasonable value while realising the convergence study with respect to the other. A `ngkpt` $= 5 \times 5 \times 5$ corresponding 19 k-points in the irreducible Brillouin zone (IBZ) was used for the convergence with respect to `ecut` and an `ecut` $= 28$ Ha was used for the convergence with respect to `ngkpt`. The graphs of the convergence studies are shown in appendix B and only the results are presented in the next paragraphs.

3.2.1 Convergence of the Total Energy

The tolerance criteria for the total energy per atom used in this work is maximum 0.05 mHa of difference with the asymptotic converged value. The convergence studies with respect to `ecut` and `ngkpt` are presented on the Figure B.1. It can be seen that the total energy is converged for `ecut` $= 20$ Ha and `ngkpt` $= 4 \times 4 \times 4$ corresponding to 10 k-points in the IBZ.

3.2.2 Convergence of the Lattice Parameter a

To be sure that the lattice constant a (variable `acell`) used in calculations corresponds to the material in equilibrium, the structure was relaxed. Convergence studies of `acell` with respect to `ecut` and `ngkpt` were made while allowing `acell` to be modified and taking into account the symmetry. This structural optimization use the Broyden-Fletcher-Goldfarb-Shanno minimization (BFGS) [20], modified to take into account the total energy as well as the gradients.

The tolerance criteria for the lattice parameter used in this work is maximum 0.2 % of difference with the asymptotic converged value. The graphs of the convergence studies are presented on the Figure B.2. It can be seen that `acell` is converged for every `ecut` starting from 12 Ha and for a `ngkpt` $= 3 \times 3 \times 3$ corresponding to 6 k-points in the IBZ. The relaxation started with a lattice constant $a = 4.643$ Å found on the Materials Project (MP) [21] which is also a theoretical calculation and ended with a relaxed lattice constant $a = 4.483$ Å. This difference can be explained by the difference of approximations used in both calculations. First the Materials Project used the projector augmented wave (PAW) method [22] for pseudopotentials and we used HGH norm-conserving ones [18]. Secondly the approximation for the exchange-correlation potential is also different, MP used the GGA PBE approximation [23] and as said before in this work the LDA is used. The latter difference explains the small variation of lattice parameters a, indeed the LDA usually underestimates a while the GGA overestimates it. The correct value is probably located somewhere between them.

3.3 Band Structure Calculation

From this we computed the band structure of PbTe. The calculations were performed at the relaxed lattice constant $a = 4.483$ Å, a cut-off of 20 Ha for the plane wave basis and a $4 \times 4 \times 4$ grid of k-points in the Brillouin zone, leading to converged results (see above). The band structure corresponds to how energy curves vary along different symmetry points in Brillouin Zone. The chosen path links the high symmetry k-points $\Gamma - X - W - K - \Gamma - L - U - W - L - K | U - X$ (see Figure 3.3). It is a common path for a FCC structure like PbTe [24] and it is then possible to compare the results with other band structure calculations found in the literature.

The band structure has been calculated without (Figure 3.4) and with (Figure 3.5) spin-orbit coupling. The valence band maximum (VBM), the conduction band minimum (CBM) and thus

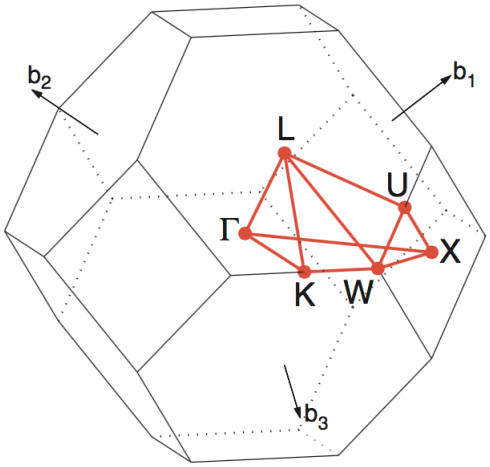

Figure 3.3: Brillouin zone of FCC lattice. High symmetry k-points path: $\Gamma - X - W - K - \Gamma - L - U - W - L - K|U - X$. (Reproduced from Setyawan [24]).

the direct band gap occur at the L point in the Brillouin zone corresponding to the point at coordinates [0.5 0.5 0.5] in the conventional (FCC) reciprocal lattice vectors.

Apart from the band gap difference (see below), the main effect of SOC can be seen on the $6p$ states of Pb, which mainly form the conduction band near the Fermi level. Due to SOC, one of the $6p$ bands splits creating new low energy curves at Γ point. Similarly the $5p$ states forming the valence band near the Fermi level also split at Γ point and lower in energy. Besides the splitting at Γ point, the effect of SOC can also be observed at L point. The $6p$ states of Pb and $5p$ states of Te forming the second and the third bands below the Fermi level are degenerate at L point. The degeneracy is removed by adding the SOC. However, the main effect of SOC on the band structure is that the p states of Pb at the conduction band minimum move downward towards the Fermi level, resulting in significantly reduced band gap at L point.

The calculated band gaps without and with SOC are given in Table 3.1, compared with the experimentally measured one. The latter increases linearly with temperature for $T \leq 400$ K and remains constant for $T > 400$ K [25]. The comparison of the band gap values shows that our calculated band gap including SOC is closer to the experimental value than calculations without SOC. However the calculated band gap including SOC is smaller than the experimental one due to the DFT band gap problem [26] (systematic underestimation of the band gaps by 30 to 50%). It is possible to predict a more precise band gap using Green's functions and in particular the *GW approximation* in the many-body perturbation theory but it is not the purpose of this work. Therefore further in this work we used the experimental band gap with its temperature dependence with the assumption of rigid bands. This means that the shape of the band structure does not change with temperature but that a shift of the conduction bands is made to fit the T dependent band gap.

In conclusion in this chapter we introduced lead telluride and its general properties as crystal structure, how it can be doped, the presence of spin-orbit interaction and how it is then taken into account in calculations. We specified our choice of pseudopotentials according to our needs and realised the convergence studies to finally be able to simulate the band structure. In Chapter 6 this band structure is used in the BoltzTraP program in order to calculate the transport coefficients.

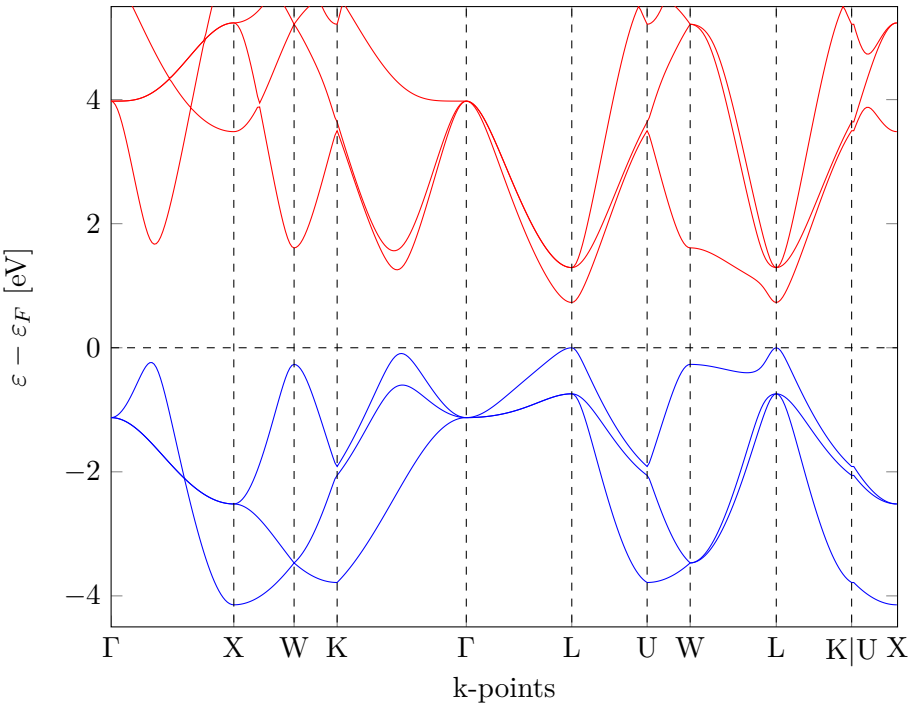

Figure 3.4: Band structure of PbTe without spin-orbit coupling. Only bands close to the Fermi level are represented. A good agreement with other calculations realised without SOC is found [21].

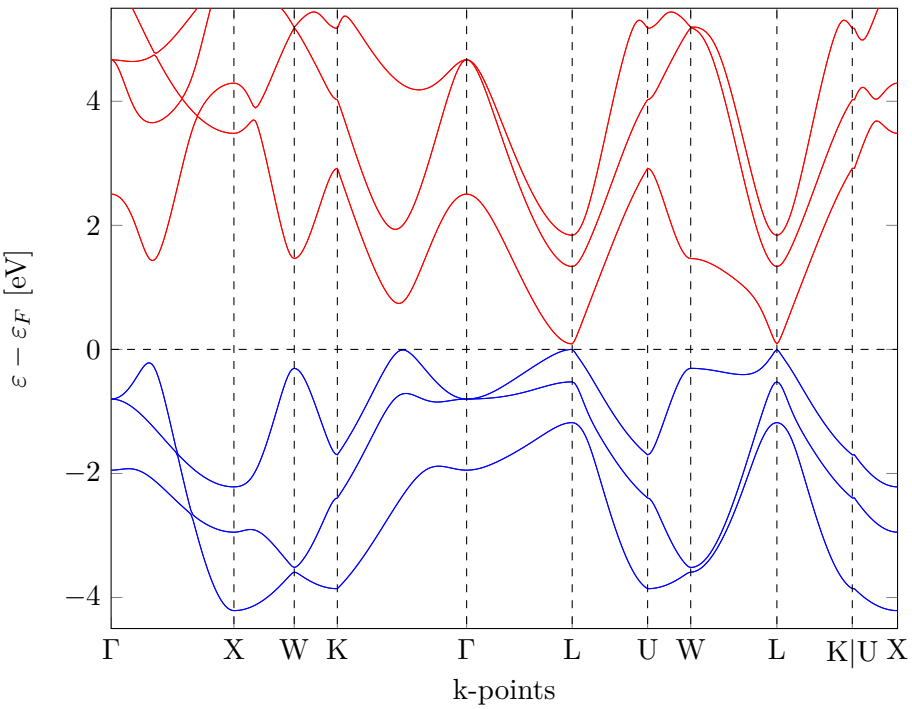

Figure 3.5: Band structure of PbTe with spin-orbit coupling. Only bands close to the Fermi level are represented.

Table 3.1: Comparison of the calculated bang gaps and the T dependent experimental value. *SOC* or *no SOC* indicates if the calculation take the spin-orbit coupling into account or not.

	LDA HGH[a]		GGA PAW[b]	Experimental[c]	
	no SOC	*SOC*	*no SOC*		
E_g [eV]	0.730	0.089	0.807	$0.19 + (0.42 \times 10^{-3})T$	$T \leq 400$ K
				0.358	$T > 400$ K

[a] This work
[b] Reference [21]
[c] Reference [25]

Chapter 4

Boltzmann Transport Theory

Contents

Non-equilibrium processes associated with charge carrier motion in a crystal under external perturbations such as an electric field, a temperature gradient, a magnetic field, etc. are referred to as electron transport phenomena or kinetic effects. They include electric conductivity, thermal conductivity, thermoelectric effect, etc. If the values governing transport phenomena, i.e., electric current density, heat flux, electric charge density, etc. do not depend on time, the charge or energy transport process is referred to as stationary. In this work, only stationary transport phenomena will be discussed. In the semi-classical case, the Boltzmann Transport Equation (BTE) for a non-equilibrium charge carrier distribution function f which accounts for the interaction with a crystal lattice is used to construct a microscopic theory of transport phenomena.

4.1 Derivation of the Boltzmann Transport Equation

This section was inspired by Ref. [27].

The conduction electrons[1] at thermodynamic equilibrium are described by the equilibrium Fermi-Dirac distribution function

$$f_0(\boldsymbol{k}) = \left\{1 + \exp\left(\frac{\varepsilon(\boldsymbol{k}) - \mu}{k_B T}\right)\right\}^{-1} \tag{4.1}$$

In the presence of an external electric field, temperature or concentration gradients, or other effects, the electron gas is in a nonequilibrium state; therefore it cannot be described by an equilibrium distribution function $f_0(\boldsymbol{k})$. In a quasiclassical approximation or in the nonequilibrium case, the distribution function $f(\boldsymbol{r}, \boldsymbol{k}, t)$ can be introduced while giving it a physical meaning, namely the local concentration near a point $\boldsymbol{r}$ at time t of electrons in the $\boldsymbol{k}$ state. To find the total number of carriers we simply add up the carriers in each momentum state. The average carrier density is

[1] For simplicity this subject is discussed as applied to the conduction electrons only but the electron holes gas can be similarly considered.

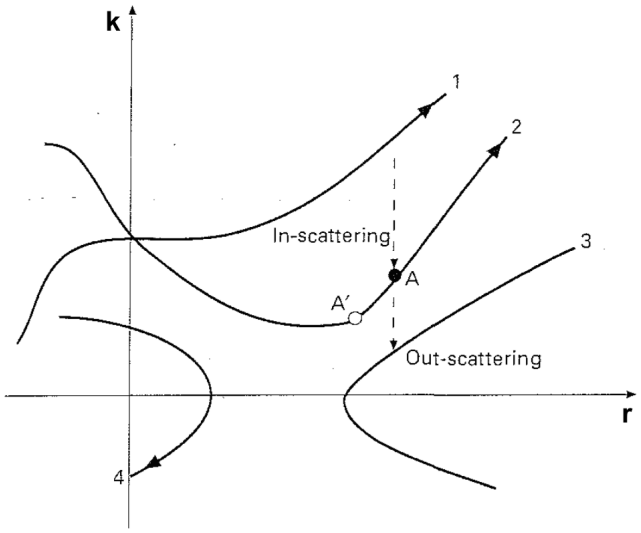

Figure 4.1: Trajectories of charge carriers in position-momentum space. Carrier's move along a trajectory according to Newton's Laws. Occasionally they scatter to another trajectory. Scattering instantly changes the carrier's momentum, but does not affect its position. (Adapted from Lundstrom [28]).

$$n(\boldsymbol{r},t) = \frac{1}{V}\sum_{\boldsymbol{k}} f(\boldsymbol{r},\boldsymbol{k},t) = \frac{1}{(2\pi)^3}\int f(\boldsymbol{r},\boldsymbol{k},t)d\boldsymbol{k} \tag{4.2}$$

Similarly we find the electron current density by weighting the sum by velocity,

$$\boldsymbol{j}(\boldsymbol{r},t) = -\frac{2e}{V}\sum_{\boldsymbol{k}} v(\boldsymbol{k})f(\boldsymbol{r},\boldsymbol{k},t) = -\frac{2e}{(2\pi)^3}\int v(\boldsymbol{k})f(\boldsymbol{r},\boldsymbol{k},t)d\boldsymbol{k} \tag{4.3}$$

In the Eq. (4.2) and (4.3), the factor 2 appears due to electron spin. If in Eq. (4.3) $f(\boldsymbol{r},\boldsymbol{k},t)$ is replaced by $f_0(\boldsymbol{k}) = f_0(\varepsilon(\boldsymbol{k}))$, then due to the energy evenness $\varepsilon(\boldsymbol{k}) = \varepsilon(-\boldsymbol{k})$ and velocity oddness $v(-\boldsymbol{k}) = -v(\boldsymbol{k})$, the electric current is equal to zero, i.e., in the equilibrium state there are no currents.

By definition, the nonequilibrium distribution function $f(\boldsymbol{r},\boldsymbol{k},t)$ is the number of electrons which at time t are in a unit volume near the point $\boldsymbol{r}$ and have a wave vector $\boldsymbol{k}$. Their number can vary due to the following three physical processes: diffusion associated with temperature or concentration gradients, leading to a variation with respect to $\boldsymbol{r}$; acceleration by external fields causing a variation of the wave electron vector $\boldsymbol{k}$; electron scattering by phonons or by other lattice defects which also cause a variation in $\boldsymbol{k}$ (see Figure 4.1).

The total effect of all these processes must be equal to the distribution function variation per unit time

$$\frac{\partial f}{\partial t} = \frac{\partial f}{\partial t}\Big|_{\text{diff}} + \frac{\partial f}{\partial t}\Big|_{\text{field}} + \frac{\partial f}{\partial t}\Big|_{\text{scatt}} \tag{4.4}$$

This is a symbolic writing of the Boltzmann transport equation where the terms of the right-hand side correspond to the variation rate due to the above processes. The BTE is an equation for f, much like a continuity equation for carriers in a 6-dimensional space, or phase space. It accounts for all possible mechanism by which f may change. In order to find an explicit form of the Boltzmann equation we shall consider these processes separately.

In the presence of a temperature or concentration gradient diffusion takes place in the conductor, therefore the charge carriers arrive at the spacial region near the point $\boldsymbol{r}$ and then leave it. The velocity of electron with wave vector $\boldsymbol{k}$ is $\boldsymbol{v}(\boldsymbol{k}) = \hbar^{-1}\boldsymbol{\nabla}_{\boldsymbol{k}}\varepsilon(\boldsymbol{k})$. The concentration of

these $\boldsymbol{k}$-electrons near the point $\boldsymbol{r}$ at time t is $f(\boldsymbol{r}, \boldsymbol{k}, t)$. After a time interval Δt, these electrons will be near the point $\boldsymbol{r} + \Delta\boldsymbol{r}$, acquiring the concentration $f(\boldsymbol{r} + \Delta\boldsymbol{r}, \boldsymbol{k}, t + \Delta t)$. In accordance with the Liouville theorem on the invariance of the phase space volume, the charge carrier concentration in the region of the point $\boldsymbol{r}$ at time t is equal to their concentration in the region of the point $\boldsymbol{r} + \Delta\boldsymbol{r}$ at time $t + \Delta t$, i.e.,

$$f(\boldsymbol{r}, \boldsymbol{k}, t) = f(\boldsymbol{r} + \Delta\boldsymbol{r}, \boldsymbol{k}, t + \Delta t) \tag{4.5}$$

By taking the Taylor expansion up to first order of the right-hand side close to $\boldsymbol{r}$, inserting $\Delta\boldsymbol{r} = \boldsymbol{v}(\boldsymbol{k})\Delta t$ and making $\Delta t \to 0$, we obtain

$$\frac{\partial f}{\partial t}\Big|_{\text{diff}} = -\boldsymbol{v}(\boldsymbol{k}) \cdot \frac{\partial f}{\partial \boldsymbol{r}} = -\boldsymbol{v}(\boldsymbol{k}) \cdot \boldsymbol{\nabla}_{\boldsymbol{r}} f \tag{4.6}$$

for the rate of the nonequilibrium distribution function variation because of diffusion.

The external force $\boldsymbol{F}$ accelerating the electrons modifies their wave vector such that $(\partial\boldsymbol{k}/\partial t) = \hbar^{-1}\boldsymbol{F}$, and consequently the number of $\boldsymbol{k}$-electrons near the point $\boldsymbol{r}$. If the same considerations as for the diffusion term are used for the $\boldsymbol{k}$-space it is possible to write

$$f(\boldsymbol{r}, \boldsymbol{k}, t) = f(\boldsymbol{r}, \boldsymbol{k} + \Delta\boldsymbol{k}, t + \Delta t) \tag{4.7}$$

which leads to

$$\frac{\partial f}{\partial t}\Big|_{\text{field}} = -\frac{\partial \boldsymbol{k}}{\partial t} \cdot \frac{\partial f}{\partial \boldsymbol{k}} = -\hbar^{-1}\boldsymbol{F} \cdot \boldsymbol{\nabla}_{\boldsymbol{k}} f \tag{4.8}$$

for the rate of variation of $f(\boldsymbol{r}, \boldsymbol{k}, t)$ owing to the external force $\boldsymbol{F}$.

For a semiconductor in an external electric field $\boldsymbol{E}$ and magnetic field $\boldsymbol{B}$, the Lorentz force acting on an electron of charge $-e$ is

$$\boldsymbol{F} = -e\left(\boldsymbol{E} + \boldsymbol{v}(\boldsymbol{k}) \times \boldsymbol{B}\right) \tag{4.9}$$

In this work only the case without magnetic field will be discussed ($\boldsymbol{B} = 0$). The Bolztmann equation for conduction electrons take thus the form

$$\frac{\partial f}{\partial t} + \boldsymbol{v}(\boldsymbol{k}) \cdot \boldsymbol{\nabla}_{\boldsymbol{r}} f - \frac{e}{\hbar}\boldsymbol{E} \cdot \boldsymbol{\nabla}_{\boldsymbol{k}} f = \frac{\partial f}{\partial t}\Big|_{\text{scatt}} \tag{4.10}$$

In order to find $(\partial f/\partial t)|_{\text{scatt}}$ we shall introduce a function $W_{\boldsymbol{k}\boldsymbol{k}'}$, which is the per-unit-time probability of electron transition from the state $\boldsymbol{k}$ to the state $\boldsymbol{k}'$ as a result of scattering by a lattice defect or phonons. The transitions from state $\boldsymbol{k}$ to every possible $\boldsymbol{k}'$ states will take place if there is an electron in the $\boldsymbol{k}$-state (probability $f(\boldsymbol{k})$) and if the $\boldsymbol{k}'$-states are vacant due Pauli's exclusion principle (probability $[1 - f(\boldsymbol{k}')]$). Therefore, because of the transitions $\boldsymbol{k} \to \boldsymbol{k}'$ the number of $\boldsymbol{k}$-electrons decreases, i.e. leaving the $\boldsymbol{k}$-state, in unit time by

$$\sum_{\boldsymbol{k}'} W_{\boldsymbol{k}\boldsymbol{k}'} f(\boldsymbol{k})(1 - f(\boldsymbol{k}')). \tag{4.11}$$

Similarly the number of $\boldsymbol{k}$-electrons, i.e., the function $f(\boldsymbol{r}, \boldsymbol{k})$ increases due to electron transition from every possible $\boldsymbol{k}'$-states to the $\boldsymbol{k}$-state by

$$\sum_{\boldsymbol{k}'} W_{\boldsymbol{k}'\boldsymbol{k}} f(\boldsymbol{k}')(1 - f(\boldsymbol{k})). \tag{4.12}$$

per unit time. The difference between the number of electrons arriving and those leaving gives the rate of variation of the nonequilibrium distribution function

$$\frac{\partial f}{\partial t}\Big|_{\text{scatt}} = \sum_{\boldsymbol{k}'} \left\{W_{\boldsymbol{k}'\boldsymbol{k}} f(\boldsymbol{k}')[1 - f(\boldsymbol{k})] - W_{\boldsymbol{k}\boldsymbol{k}'} f(\boldsymbol{k})[1 - f(\boldsymbol{k}')]\right\} \tag{4.13}$$

Replacing the sums in the collisions terms by integrals we obtain

$$\frac{\partial f}{\partial t}\Big|_{\text{scatt}} = -\int \frac{d\boldsymbol{k}'}{(2\pi)^3} \left\{ W_{\boldsymbol{k}\boldsymbol{k}'} f(\boldsymbol{k}) \left[1 - f(\boldsymbol{k}')\right] - W_{\boldsymbol{k}'\boldsymbol{k}} f(\boldsymbol{k}') \left[1 - f(\boldsymbol{k})\right] \right\} \tag{4.14}$$

As mentioned before, in this work we considered only the stationary case when the external fields do not explicitly depend on time and, consequently, $\partial f/\partial t = 0$. In the stationary case, from Eqs. (4.10) and (4.14) we can obtain an explicit form of the Boltzmann equation for the conduction electrons in electric field:

$$\boldsymbol{v}(\boldsymbol{k}) \cdot \boldsymbol{\nabla}_{\boldsymbol{r}} f(\boldsymbol{r}, \boldsymbol{k}) - \frac{e}{\hbar} \boldsymbol{E} \cdot \boldsymbol{\nabla}_{\boldsymbol{k}} f(\boldsymbol{r}, \boldsymbol{k}) = -\int \frac{d\boldsymbol{k}'}{(2\pi)^3} \Big(W_{\boldsymbol{k}\boldsymbol{k}'} f(\boldsymbol{r}, \boldsymbol{k}) \left[1 - f(\boldsymbol{r}, \boldsymbol{k}')\right] - W_{\boldsymbol{k}'\boldsymbol{k}} f(\boldsymbol{r}, \boldsymbol{k}') \left[1 - f(\boldsymbol{r}, \boldsymbol{k})\right] \Big) \tag{4.15}$$

The BTE (4.15) is therefore an integro-differential equation. The function $W_{\boldsymbol{k}\boldsymbol{k}'}$ entering into the collision part of the Boltzmann equation depends on the nature of the conduction electron scattering process, and for a particular mechanism it is governed by the quantum theory of scattering. Thus, the major problem of the transport theory is reduced to two independent problems, namely the calculation of $W_{\boldsymbol{k}\boldsymbol{k}'}$ for different scattering mechanisms and the solution of the Boltzmann Equation (4.15) in order to find the nonequilibrium distribution function $f(\boldsymbol{r}, \boldsymbol{k}, t)$.

4.2 Relaxation Time Approximation

The previous section showed that in the general case the Boltzmann Transport Equation is a rather complicated non linear integro-differential equation for $f(\boldsymbol{r}, \boldsymbol{k}, t)$. To find a solution of the BTE in practice, some simplifying approximations are needed. A commonly used simplification for the collision term of Eq. (4.14) is called the *Relaxation Time Approximation* (RTA). In the following section, we explore solutions to the BTE using this simplification.

First according to the principle of detailed equilibrium, in the state of equilibrium where $f(\boldsymbol{r}, \boldsymbol{k}, t) = f_0(\boldsymbol{k})$, in unit time the number of electrons coming into the $\boldsymbol{k}$-state from the $\boldsymbol{k}'$-state is equal to the number of electrons coming out from the $\boldsymbol{k}$-state into the $\boldsymbol{k}'$ state:

$$W_{\boldsymbol{k}\boldsymbol{k}'} f_0(\boldsymbol{k})[1 - f_0(\boldsymbol{k}')] = W_{\boldsymbol{k}'\boldsymbol{k}} f_0(\boldsymbol{k}')[1 - f_0(\boldsymbol{k})] \tag{4.16}$$

Let us continue by writing the non-equilibrium distribution function as

$$f(\boldsymbol{r}, \boldsymbol{k}, t) = f_0(\boldsymbol{r}, \boldsymbol{k}) + \delta f(\boldsymbol{r}, \boldsymbol{k}) \tag{4.17}$$

where $f_0(\boldsymbol{r}, \boldsymbol{k})$ is the local equilibrium function close to Eq. (4.1) but with the local chemical potential and temperature

$$f_0(\boldsymbol{r}, \boldsymbol{k}) = \left\{ 1 + \exp\left(\frac{\varepsilon(\boldsymbol{k}) - \mu(\boldsymbol{r})}{k_B T(\boldsymbol{r})} \right) \right\}^{-1} \tag{4.18}$$

and $\delta f(\boldsymbol{r}, \boldsymbol{k})$ is a non-equilibrium supplement to be defined. It is obvious that $\delta f(\boldsymbol{r}, \boldsymbol{k})$ is an odd function of $\boldsymbol{k}$ while $f_0(\boldsymbol{r}, \boldsymbol{k})$ is an even function of $\boldsymbol{k}$. In addition, $\delta f(\boldsymbol{r}, \boldsymbol{k})$ must be proportional to the electric field and the temperature gradient, since these forces result in a deviation from the equilibrium conduction electron distribution in the $\boldsymbol{k}$ state. Almost in all real cases the deviation from equilibrium is small, i.e.,

$$|\delta f| = |f - f_0| \ll f_0 \tag{4.19}$$

Let us make the assumption that $W_{\boldsymbol{k}\boldsymbol{k}'}$ is one and the same for both equilibrium and non-equilibrium states. This is true in the absence of quantization, when $W_{\boldsymbol{k}\boldsymbol{k}'}$ does not depend on the magnetic and electric field nor the temperature gradient [27].

Let us substitute Eq. (4.17) into Eq. (4.14) and use Eq. (4.16). Accounting for Eq. (4.19) we keep only linear terms in $\delta f(\boldsymbol{k})$. We obtain:

$$\frac{\partial f}{\partial t}\Big|_{scatt} = -\frac{\delta f(\boldsymbol{k})}{\tau(\boldsymbol{k})} \tag{4.20}$$

where $\tau(\boldsymbol{k})$ is called the *relaxation time* and is defined as:

$$\frac{1}{\tau(\boldsymbol{k})} = \int \frac{d\boldsymbol{k}'}{(2\pi)^3} W_{\boldsymbol{k}\boldsymbol{k}'} \left(\frac{1 - f_0(\boldsymbol{k}')}{1 - f_0(\boldsymbol{k})} - \frac{f_0(\boldsymbol{k})}{f_0(\boldsymbol{k}')} \frac{\delta f(\boldsymbol{k}')}{\delta f(\boldsymbol{k})} \right) \tag{4.21}$$

The name relaxation time can be explained as follows. Assume that the external forces perturb the equilibrium of the conduction electron system. If at time $t = 0$ the external field is switched off, $\boldsymbol{F} = 0$, and the temperature gradient is cancelled, $\boldsymbol{\nabla}_{\boldsymbol{r}} f = 0$, the nonequilibrium function $f(\boldsymbol{r}, \boldsymbol{k}, t)$ will tend to an equilibrium function $f_0(\boldsymbol{k})$. In this case $f(\boldsymbol{r}, \boldsymbol{k}, t)$ satisfies the equation

$$\frac{\partial f(\boldsymbol{r}, \boldsymbol{k}, t)}{\partial t} + \frac{f(\boldsymbol{r}, \boldsymbol{k}, t) - f_0(\boldsymbol{r}, \boldsymbol{k})}{\tau(\boldsymbol{k})} = 0 \tag{4.22}$$

From Eq. (4.22) we obtain the following law of the nonequilibrium function variation,

$$(f - f_0)_t = (f - f_0)_{t=0} \exp(-t/\tau) \tag{4.23}$$

It is seen that the relaxation time τ characterizes the speed of recovery of the equilibrium state.

Substituting Eq. (4.20) into the right-hand side of Eq. (4.15) we obtain the following simple form of the stationary Boltzmann equation in the absence of a magnetic field,

$$\boldsymbol{v}(\boldsymbol{k}) \cdot \boldsymbol{\nabla}_{\boldsymbol{r}} f(\boldsymbol{r}, \boldsymbol{k}) - \frac{e}{\hbar} \boldsymbol{E} \cdot \boldsymbol{\nabla}_{\boldsymbol{k}} f(\boldsymbol{r}, \boldsymbol{k}) = -\frac{f(\boldsymbol{r}, \boldsymbol{k}) - f_0(\boldsymbol{r}, \boldsymbol{k})}{\tau(\boldsymbol{k})} \tag{4.24}$$

Thus, by introducing the notion of relaxation time we formally reduce the integro-differential Equation (4.15) to the differential Equation (4.24) for the nonequilibrium distribution function $f(\boldsymbol{r}, \boldsymbol{k})$. However, in the general case this is a seeming simplification of the Boltzmann equation. Indeed, the ratio of two values of the unknown function δf enters into the right-hand side of Eq. (4.24) in terms of $\tau(\boldsymbol{k})$ (Eq. (4.21)) under the integration sign. In the case where the ratio $\delta f(\boldsymbol{k}')/\delta f(\boldsymbol{k})$ does not depend on both the type and magnitude of the disturbance (electric field or temperature gradient) the value $\tau(\boldsymbol{k})$ is a characteristic of the conductor and has a reasonable physical sense.

4.3 Calculation of Transport Coefficients

This section aims to show how the transport coefficients can be computed from the Boltzamnn Transport Equation when using the Relaxation Time Approximation.

The local equilibrium distribution function $f_0(\boldsymbol{r}, \boldsymbol{k})$ is given by

$$f_0(\boldsymbol{r}, \boldsymbol{k}) = \left\{ 1 + \exp\left(\frac{\varepsilon(\boldsymbol{k}) - \mu(\boldsymbol{r})}{k_B T(\boldsymbol{r})} \right) \right\}^{-1} \tag{4.25}$$

Let us first compute the differential of f_0,

$$
\begin{aligned}
df_0 &= k_B T \frac{\partial f_0}{\partial \varepsilon} d\left(\frac{\varepsilon-\mu}{k_B T}\right) \\
&= k_B T \frac{\partial f_0}{\partial \varepsilon}\left\{-\frac{d\mu}{k_B T} - \frac{(\varepsilon-\mu)dT}{k_B T^2} + \frac{d\varepsilon}{k_B T}\right\} \\
&= -\frac{\partial f_0}{\partial \varepsilon}\left\{\frac{\partial \mu}{\partial \boldsymbol{r}}\cdot d\boldsymbol{r} + \frac{\varepsilon-\mu}{T}\frac{\partial T}{\partial \boldsymbol{r}}\cdot d\boldsymbol{r} - \frac{\partial \varepsilon}{\partial \boldsymbol{k}}\cdot d\boldsymbol{k}\right\}
\end{aligned} \tag{4.26}
$$

from which it comes that

$$
\frac{\partial f_0}{\partial \boldsymbol{r}} = \left\{\frac{\partial \mu}{\partial \boldsymbol{r}} + \frac{\varepsilon-\mu}{T}\frac{\partial T}{\partial \boldsymbol{r}}\right\}\left(-\frac{\partial f_0}{\partial \varepsilon}\right) \tag{4.27}
$$

$$
\frac{\partial f_0}{\partial \boldsymbol{k}} = \hbar \boldsymbol{v}\frac{\partial f_0}{\partial \varepsilon} \tag{4.28}
$$

Using these relations, if Eq. (4.17) is substituted in Eq. (4.24) and by keeping only the function $f_0(\boldsymbol{r},\boldsymbol{k})$ on the right-hand side, we obtain the linearised stationary Boltzmann equation

$$
\begin{aligned}
-\frac{f(\boldsymbol{r},\boldsymbol{k}) - f_0(\boldsymbol{r},\boldsymbol{k})}{\tau(\boldsymbol{k})} &= \boldsymbol{v}\cdot\frac{\partial f_0}{\partial \boldsymbol{r}} - \frac{e}{\hbar}\boldsymbol{E}_0\cdot\frac{\partial f_0}{\partial \boldsymbol{k}} \\
&= \boldsymbol{v}\cdot\left[\frac{\partial \mu}{\partial \boldsymbol{r}} + \frac{\varepsilon-\mu}{T}\frac{\partial T}{\partial \boldsymbol{r}}\right]\left(-\frac{\partial f_0}{\partial \varepsilon}\right) - e\boldsymbol{E}_0\cdot\boldsymbol{v}\frac{\partial f_0}{\partial \varepsilon} \\
&= \boldsymbol{v}\cdot\left[\frac{\partial \mu}{\partial \boldsymbol{r}} + e\boldsymbol{E}_0 + \frac{\varepsilon-\mu}{T}\boldsymbol{\nabla}_{\boldsymbol{r}} T\right]\left(-\frac{\partial f_0}{\partial \varepsilon}\right) \\
&= \boldsymbol{v}\cdot\left[e\boldsymbol{E} + \frac{\varepsilon-\mu}{T}\boldsymbol{\nabla}_{\boldsymbol{r}} T\right]\left(-\frac{\partial f_0}{\partial \varepsilon}\right)
\end{aligned} \tag{4.29}
$$

where $\boldsymbol{E_0}$ is the external applied electric field $\boldsymbol{E_0} = -\boldsymbol{\nabla}\phi_0$ and $\boldsymbol{E} = -\boldsymbol{\nabla}(\phi_0 - \mu/e)$ is the gradient of the electrochemical potential taking also into account the gradient of the chemical potential. Further we will refer to $\boldsymbol{E}$ as the electric field. This leads us to

$$
f(\boldsymbol{r},\boldsymbol{k}) = f_0(\boldsymbol{r},\boldsymbol{k}) - \tau(\boldsymbol{k})\boldsymbol{v}(\boldsymbol{k})\cdot\boldsymbol{\Phi}(\varepsilon,\boldsymbol{r})\left(\frac{\partial f_0(\boldsymbol{r},\boldsymbol{k})}{\partial \varepsilon}\right) \tag{4.30}
$$

$$
\implies \delta f = -\tau(\boldsymbol{k})\boldsymbol{v}(\boldsymbol{k})\cdot\boldsymbol{\Phi}(\varepsilon)\left(\frac{\partial f_0(\boldsymbol{r},\boldsymbol{k})}{\partial \varepsilon}\right) \tag{4.31}
$$

with $\boldsymbol{\Phi}(\varepsilon)$ the generalized disturbing force causing a deviation from equilibrium

$$
\boldsymbol{\Phi}(\varepsilon,\boldsymbol{r}) = -e\boldsymbol{E}(\boldsymbol{r}) - \frac{\varepsilon-\mu(\boldsymbol{r})}{T(\boldsymbol{r})}\boldsymbol{\nabla}_{\boldsymbol{r}} T(\boldsymbol{r}) \tag{4.32}
$$

It is now possible to compute transport coefficients, let us begin with the conductivity tensor. Consider a conductor with no magnetic field nor temperature gradient and with a spatially uniform electric field $\boldsymbol{E}$. Replacing Eq. (4.30) in Eq. (4.3) and taking into account that the equilibrium distribution $f_0(\boldsymbol{r},\boldsymbol{k})$ does not contribute to the current, since $f_0(\boldsymbol{r},-\boldsymbol{k}) = f_0(\boldsymbol{r},\boldsymbol{k})$, the current density is given by

$$
\begin{aligned}
j^{\alpha}(\boldsymbol{r}) &= -\frac{2e}{(2\pi)^3}\int v^{\alpha}(\boldsymbol{k}) f(\boldsymbol{r},\boldsymbol{k},t) d\boldsymbol{k} \\
&= -\frac{2e}{(2\pi)^3}\int v^{\alpha}(\boldsymbol{k})\, \delta f(\boldsymbol{r},\boldsymbol{k}) d\boldsymbol{k} \\
&= \frac{2e^2}{(2\pi)^3} E^{\beta}\int \tau(\boldsymbol{k}) v^{\alpha}(\boldsymbol{k}) v^{\beta}(\boldsymbol{k}) \left(-\frac{\partial f_0}{\partial \varepsilon}\right) d\boldsymbol{k}
\end{aligned} \tag{4.33}
$$

The conductivity tensor is defined by the linear relation $j^{\alpha} = \sigma_{\alpha\beta} E^{\beta}$. We have thus derived an expression for the conductivity tensor,

$$
\sigma_{\alpha\beta} = \frac{2e^2}{(2\pi)^3}\int \tau(\boldsymbol{k}) v^{\alpha}(\boldsymbol{k}) v^{\beta}(\boldsymbol{k}) \left(-\frac{\partial f_0}{\partial \varepsilon}\right) d\boldsymbol{k} \tag{4.34}
$$

Similar expressions can be found for other transport coefficient tensors, consider a small region of solid with a fixed volume ΔV. The first law of thermodynamics applied to this region gives $T\Delta S = \Delta E - \mu \Delta N$. Dividing by ΔV gives

$$
dq \equiv T ds = d\varepsilon - \mu dn \tag{4.35}
$$

where s is the entropy density, ε is energy density, and n the number density. This can be directly recast as the following relation among current densities

$$
\boldsymbol{j}_q = T\boldsymbol{j}_s = \boldsymbol{j}_{\varepsilon} - \mu \boldsymbol{j}_n \tag{4.36}
$$

where $\boldsymbol{j}_n = \boldsymbol{j}/(-e)$ and $\boldsymbol{j}_{\varepsilon}$ is the energy current density,

$$
\boldsymbol{j}_{\varepsilon} = \frac{2}{(2\pi)^3}\int \varepsilon\, \boldsymbol{v}\, \delta f d\boldsymbol{k} \tag{4.37}
$$

and $\boldsymbol{j}_s$ is the entropy current density. Accordingly, the thermal current density $\boldsymbol{j}_q$ is defined as

$$
\begin{aligned}
\boldsymbol{j}_q \equiv T\boldsymbol{j}_s &= \boldsymbol{j}_{\varepsilon} + \frac{\mu}{e}\boldsymbol{j} \\
&= \frac{2}{(2\pi)^3}\int \boldsymbol{v}(\varepsilon - \mu)\, \delta f d\boldsymbol{k}
\end{aligned} \tag{4.38}
$$

We now consider both the electrical current $\boldsymbol{j}$ and the thermal current density $\boldsymbol{j}_q$. One obtains

$$
\boldsymbol{j} = -\frac{2e}{(2\pi)^3}\int \boldsymbol{v}\, \delta f d\boldsymbol{k} \equiv L_{11}\boldsymbol{E} - L_{12}\boldsymbol{\nabla} T \tag{4.39}
$$

$$
\boldsymbol{j}_q = \frac{2}{(2\pi)^3}\int (\varepsilon - \mu)\boldsymbol{v}\, \delta f d\boldsymbol{k} \equiv L_{21}\boldsymbol{E} - L_{22}\boldsymbol{\nabla} T \tag{4.40}
$$

where the transport coefficients tensors L_{ij} are obtained by injecting Eq. (4.31) in the integrals above and changing the variable of integration from $\boldsymbol{k}$ to ε by the relation

$$
d\boldsymbol{k} = \frac{d\varepsilon\, d\Omega_{\varepsilon}}{|\partial\varepsilon/\partial\boldsymbol{k}|} = \frac{d\varepsilon\, d\Omega_{\varepsilon}}{\hbar|\boldsymbol{v}|} \tag{4.41}
$$

where $d\Omega_{\varepsilon}$ is the differential area on the constant energy surface $\varepsilon(\boldsymbol{k}) = \varepsilon$ [29].

This leads to

$$L_{11}^{\alpha\beta} = \frac{e^2}{4\pi^3\hbar}\int d\varepsilon\,\tau(\varepsilon)\left(-\frac{\partial f_0}{\partial\varepsilon}\right)\int d\Omega_\varepsilon \frac{v^\alpha v^\beta}{|\boldsymbol{v}|} \tag{4.42}$$

$$L_{21}^{\alpha\beta} = TL_{12}^{\alpha\beta} = -\frac{e}{4\pi^3\hbar}\int d\varepsilon\,\tau(\varepsilon)(\varepsilon-\mu)\left(-\frac{\partial f_0}{\partial\varepsilon}\right)\int d\Omega_\varepsilon \frac{v^\alpha v^\beta}{|\boldsymbol{v}|} \tag{4.43}$$

$$L_{22}^{\alpha\beta} = \frac{1}{4\pi^3\hbar T}\int d\varepsilon\,\tau(\varepsilon)(\varepsilon-\mu)^2\left(-\frac{\partial f_0}{\partial\varepsilon}\right)\int d\Omega_\varepsilon \frac{v^\alpha v^\beta}{|\boldsymbol{v}|} \tag{4.44}$$

The linear relations in Eqs. (4.39) and (4.40) can be expressed as

$$\boldsymbol{E} = \frac{1}{\sigma}\,\boldsymbol{j} + S\,\boldsymbol{\nabla}T \tag{4.45}$$

$$\boldsymbol{j}_q = \Pi\,\boldsymbol{j} - \kappa\,\boldsymbol{\nabla}T \tag{4.46}$$

where the tensors σ, S, Π and κ are given by

$$\sigma = L_{11} \qquad S = L_{11}^{-1}L_{12} \tag{4.47}$$

$$\Pi = L_{21}L_{11}^{-1} \qquad \kappa = L_{22} - L_{21}L_{11}^{-1}L_{12} \tag{4.48}$$

The names and physical interpretation of these four transport coefficient is as follows

- σ is the conductivity: $\boldsymbol{j} = \sigma\,\boldsymbol{E}$ under the condition of zero thermal gradient;
- S is the Seebeck coefficient: $\boldsymbol{E} = S\,\boldsymbol{\nabla}T$ under the condition of zero electrical current;
- Π is the Peltier coefficient: $\boldsymbol{j}_q = \Pi\,\boldsymbol{j}$ under the condition of zero thermal gradient;
- κ is the electronic thermal conductivity: $\boldsymbol{j}_q = -\kappa\,\boldsymbol{\nabla}T$ under the condition of zero electrical current. As it can be seen from Eq. (4.40), the electronic thermal conductivity when the electric field is zero is simply given by $\kappa = L_{22}$.

4.4 Solving the BTE with the BoltzTraP Program

In Chapter 6, the integrals of Eqs. (4.42) to (4.44) are calculated using the BoltzTraP code in order to compute the transport coefficients with the Eqs. (4.47) and (4.48).

BoltzTraP is an open-source program for calculating the semi-classic transport coefficients by solving the Boltzmann equation. It performs a Fourier expansion of the band energies using symmetry-conserving star functions to build a smooth analytical representation of the bands. The idea of the Fourier expansion is to use more star functions than band energies, but to constrain the fit so that the extrapolated energies are exactly equal to the calculated band-energies and use the additional freedom to minimize a roughness function and thereby suppress oscillations between the data-points [4]. Using the analytical representation of the bands it is then possible to calculate band-structure- and derivatives of band structure-dependent quantities. As explained in the next chapter, the relaxation time τ is in principle dependent on both the energy ε and temperature T. However, in BoltzTraP, the relaxation time is by default assumed to be a constant, so the program outputs only σ/τ. This is a rather crude approximation and more sophisticated models are derived in the next chapter. It also explain how we modified the code to implement these models in BoltzTraP.

Chapter 5

Relaxation Times for Different Scattering Mechanisms

Contents

In this section models of the relaxation times $\tau(\varepsilon)$ appearing in Eqs. (4.42) to (4.44) are derived for different scattering mechanisms.

As we know the scattering in a semiconductor is due to several mechanisms. The total scattering rate is expressed as a summation of different contributions: acoustic phonons (a), optical phonons with deformation coupling (o), optical phonons with polar coupling (po), vacancies (v), and Coulomb scattering from charged impurities (C),

$$\frac{1}{\tau_{\text{tot}}} = \frac{1}{\tau_{\text{v}}} + \frac{1}{\tau_{\text{C}}} + \frac{1}{\tau_{\text{a}}} + \frac{1}{\tau_{\text{o}}} + \frac{1}{\tau_{\text{po}}} \tag{5.1}$$

At low temperature for which lattice oscillations are not intensive, the phonon gas is rarefied and the scattering due to lattice point defects and ionized impurities are dominant. As the temperature increases, the number of phonons increases and consequently charge carrier scattering by phonons becomes the main relaxation mechanism. For PbTe between 300 and 900 K, it has been shown that only phonons scattering processes play a significant role in the relaxation [30]. Consequently in this work we considered only three scattering mechanisms, namely scattering by acoustic phonons (a), optical phonons with deformation coupling (o) and optical phonons with polar coupling (po)

$$\frac{1}{\tau_{\text{tot}}} \simeq \frac{1}{\tau_{\text{a}}} + \frac{1}{\tau_{\text{o}}} + \frac{1}{\tau_{\text{po}}} \tag{5.2}$$

The simpler and most used model is to consider a constant relaxation time τ being a inherent property of each material. However as shown in the next chapter, it is a crude approximation that does not fit with experimental results for most transport coefficients. More sophisticated models with energy and temperature dependence $\tau(\varepsilon, T)$ are derived below.

Although the theoretical band structure of PbTe has been calculated with ABINIT in Chapter 3, in this chapter we consider an arbitrary spherically symmetric band structure, i.e. the energy of the charge carriers, ε being an arbitrary function of the wave vector magnitude $|\boldsymbol{k}|$

$$\varepsilon(\boldsymbol{k}) = \varepsilon(k) \tag{5.3}$$

This simplification is necessary to derive an expression for the relaxation time usable in practice and even though it is not totally exact, it is a sufficient approximation for approaching the relaxation time in case of highly symmetric materials like PbTe.

Let us start from the Eq. (4.21) for the relaxation time derived above. By injecting Eq. (4.31) in it and taking into account that

$$f_0(\boldsymbol{k})(1 - f_0(\boldsymbol{k})) = -k_B T \left(\frac{\partial f_0(\boldsymbol{k})}{\partial \varepsilon} \right) \tag{5.4}$$

we obtain for the relaxation time

$$\frac{1}{\tau(\boldsymbol{k})} = \int \frac{d\boldsymbol{k}'}{(2\pi)^3} W_{\boldsymbol{k}\boldsymbol{k}'} \frac{1 - f_0(\varepsilon')}{1 - f_0(\varepsilon)} \left(1 - \frac{\tau(\boldsymbol{k}')\boldsymbol{v}(\boldsymbol{k}') \cdot \boldsymbol{\Phi}(\varepsilon')}{\tau(\boldsymbol{k})\boldsymbol{v}(\boldsymbol{k}) \cdot \boldsymbol{\Phi}(\varepsilon)} \right) \tag{5.5}$$

From the symmetric dispersion relation defined in Eq. (5.3) it follows that the scattering time must be isotropic and will thus depend only on the magnitude $k = |\boldsymbol{k}|$. Moreover, in the case of isotropic bands, the directions of the electron velocity $\boldsymbol{v}$ and wave vector $\boldsymbol{k}$ coincide and we have

$$\boldsymbol{v}(\boldsymbol{k}) = \frac{\hbar \boldsymbol{k}}{m(k)} \tag{5.6}$$

where $m(k)$ is the effective electron mass.

If we also constrain this work to the case where the scattering is elastic $\varepsilon' = \varepsilon(\boldsymbol{k}') = \varepsilon(\boldsymbol{k}) = \varepsilon(k)$ and consequently $k = k'$, i.e. the charge carriers exchange only impulses, $\tau(k)$ becomes a universal function characterizing the system relaxation. The assumption of elasticity is generally speaking not valid for phonons scattering but at sufficiently high temperature when the carrier energy is much larger than the phonon energy, the collisions are almost elastic and the phonon energy can be neglected [27].

Taking this in consideration and injecting Eq. (5.6) in Eq. (5.5) the relaxation time expression simply becomes

$$\frac{1}{\tau(k)} = \int \frac{d\boldsymbol{k}'}{(2\pi)^3} W_{\boldsymbol{k}\boldsymbol{k}'} \left(1 - \frac{\boldsymbol{k}' \cdot \boldsymbol{\Phi}(\varepsilon)}{\boldsymbol{k} \cdot \boldsymbol{\Phi}(\varepsilon)} \right) \tag{5.7}$$

In spherical coordinates, if the polar axis is directed along $\boldsymbol{k}$ and the polar angles of the vectors $\boldsymbol{k}'$ and $\boldsymbol{\Phi}(\varepsilon)$ are denoted by (θ, ϕ) and (α, β) respectively, we have

$$\cos(\boldsymbol{k}', \boldsymbol{\Phi}(\varepsilon)) = \cos\phi \cos\beta + \sin\phi \sin\beta \cos(\theta - \alpha) \tag{5.8}$$

and

$$\cos(\boldsymbol{k}, \boldsymbol{\Phi}(\varepsilon)) = \cos\beta \tag{5.9}$$

This leads to

$$\frac{1}{\tau(k)} = \int \frac{d\boldsymbol{k}'}{(2\pi)^3} W_{\boldsymbol{k}\boldsymbol{k}'} \left(1 - \cos\phi - \sin\phi \tan\beta \cos(\theta - \alpha)\right) \tag{5.10}$$

When performing the integral in $\boldsymbol{k}'$, the $\sin\phi$ dependent term yields zero and the relaxation time is then given by

$$\frac{1}{\tau(k)} = \int \frac{d\boldsymbol{k}'}{(2\pi)^3} W_{\boldsymbol{k}\boldsymbol{k}'} \left(1 - \cos\phi\right)$$

$$= \int \frac{d\boldsymbol{k}'}{(2\pi)^3} W_{\boldsymbol{k}\boldsymbol{k}'} \left(1 - \frac{\boldsymbol{k}\cdot\boldsymbol{k}'}{k^2}\right) \tag{5.11}$$

To summarize, the simple expression of Eq. (5.11) is valid under the three approximations made above, namely the smallness of deviation from equilibrium (see Eq. (4.19)), the isotropy of the band structure (Eq. (5.3)) and the elasticity of the scattering $\varepsilon = \varepsilon'$.

5.1 Transition Probability

Non-stationary perturbation theory allows us to define the transition probability $W_{\boldsymbol{k}\boldsymbol{k}'}$. In this theory, the Hamiltonian is expressed as a sum of the Hamiltonian of the unperturbed system $\hat{\mathcal{H}}$ and a small perturbation $\hat{\mathcal{H}}'$ describing the interaction of the electron with phonons.

$$\hat{\mathcal{H}}_T = \hat{\mathcal{H}} + \hat{\mathcal{H}}' \tag{5.12}$$

Using this theory in the first order of perturbation and making the assumptions of a small disturbance magnitude acting in a short time compared to the time between two successive perturbations, it can be shown (see Ref. [27]) that the transition probability takes the form

$$W_{\boldsymbol{k}\boldsymbol{k}'} = \frac{2\pi}{\hbar} \left|(\boldsymbol{k}'|\hat{\mathcal{H}}'|\boldsymbol{k})\right|^2 \delta(\varepsilon_{k'} - \varepsilon_k) \tag{5.13}$$

This expression is then used in Eq. (5.11) in order to find the different relaxation times.

5.2 Acoustic Phonons Scattering

PbTe (and more generally all solids with more than one atom in the smallest unit cell) exhibits two types of phonons: acoustic phonons and optical phonons.

Acoustic phonons correspond to in-phase movements of lattice atoms out of their equilibrium positions. If the displacements are in the same direction as the propagation of the wave, then some atoms will be closer and some others will be farther apart. This is the same principle as a sound wave, hence the name *acoustic* phonons. Transversal waves are comparable to waves in water. For long wavelength, acoustic phonons exhibit a linear relation between wavevector and frequency and for very long wavelength, the frequencies of acoustic phonons tend to zero [31].

When an elastic wave propagates in a crystal, the primitive cell, being deformed, changes its volume (the lattice constant changes), which results in a variation of the positions of the conduction band minimum (CBM) and the valence band maximum (VBM) as the band width is sensitive to the lattice constant value. This shift in the band edges corresponds to the energy of the interaction of charge carriers with lattice oscillations. This energy is called the deformation potential and is related to the displacement of the lattice ions by

$$\hat{\mathcal{H}}'_{\mathrm{a}} = E_{\mathrm{a}} \operatorname{div} \boldsymbol{u}_{\mathrm{a}}(\boldsymbol{r}) \tag{5.14}$$

where $\boldsymbol{u}_{\mathrm{a}}(\boldsymbol{r})$ is the shift of position of the ions and E_{a} is called the deformation potential constant [32].

Following the work of B.M. Askerov (Ref. [27]), and again with the hypothesis of arbitrary isotropic (spherically symmetric) bands and elastic scattering, the transition probability from $\boldsymbol{k}$ to $\boldsymbol{k}'$ writes

$$W^{\mathrm{a}}_{\boldsymbol{k}\boldsymbol{k}'} = \frac{2\pi}{MN}\frac{E_{\mathrm{a}}^2}{\hbar\, v_0^2} k_B T\, \delta(\varepsilon_{\boldsymbol{k}'} - \varepsilon_{\boldsymbol{k}}) \tag{5.15}$$

where M is the mass of one ion, N is the total number of it and v_0 is the sound velocity in the crystal.

Replacing this expression in Eq. (5.11) leads to

$$\frac{1}{\tau(k)} = \frac{2\pi}{MN}\frac{E_{\mathrm{a}}^2}{\hbar\, v_0^2} k_B T \int \frac{d\boldsymbol{k}'}{(2\pi)^3}\left(1 - \frac{\boldsymbol{k}\cdot\boldsymbol{k}'}{k^2}\right)\delta(\varepsilon_{\boldsymbol{k}'} - \varepsilon_{\boldsymbol{k}}) \tag{5.16}$$

Hence, it follows that in the integration over $\boldsymbol{k}'$ the second term yields zero. Consequently, in the elastic approximation the transition from any $\boldsymbol{k}'$-state to the $\boldsymbol{k}$-state does not contribute to the relaxation time. If in the integral the volume elements in the $\boldsymbol{k}'$-space are written in spherical coordinates, the integral over angles will yield 4π while the integral over the magnitude $\boldsymbol{k}'$ can be taken using δ-functions. As a result, we obtain for the relaxation time for scattering by acoustic phonons

$$\tau_{\mathrm{a}}(k,T) = \frac{\pi\hbar\rho}{E_{\mathrm{a}}^2}\frac{v_0^2}{k_B T}\frac{1}{k^2}\left(\frac{\partial\varepsilon}{\partial k}\right) \tag{5.17}$$

where $\rho = MN/V$ is the crystal density.

It could be possible to use directly this expression with the $\frac{1}{k^2}\left(\frac{\partial\varepsilon}{\partial k}\right)$ term since we calculated the band structure with ABINIT in Chapter 3, however for simplicity we used a parabolic band structure in the following in order to obtain a relaxation time directly depending of energy and temperature.

For a parabolic band (around the L point for PbTe) the dispersion relation is given by

$$\varepsilon = \frac{\hbar^2 k^2}{2m^*} \tag{5.18}$$

From this it is easy to express Eq. (5.17) in terms of energy and obtain the relaxation time for scattering by acoustical phonons in a parabolic model :

$$\tau_{\mathrm{a}}(\varepsilon,T) = \frac{2\pi\hbar^4\rho v_0^2}{E_{\mathrm{a}}^2(2m^* k_B T)^{3/2}}\left(\frac{\varepsilon}{k_B T}\right)^{-1/2} \tag{5.19}$$

In conclusion the relaxation time for scattering by acoustic phonon varies as $\tau_{\mathrm{a}}(\varepsilon,T) \sim T^{-1}\,\varepsilon^{-1/2}$ meaning that scattering becomes more important as energy and temperature increase.

5.3 Non-polar Optical Phonons Scattering

When the lattice is composed of at least two different atoms, the crystal exhibits optical phonons in addition to acoustic phonons. They corresponds to out-of-phase displacements of the atoms in the lattice, one atom moving in a direction and its neighbours in the opposite one. In the Brillouin zone center, the optical phonons have a frequency different from zero and they show little dispersion near that long wavelength limit [31]. For long-wave optical oscillations ($q \to 0$) atoms in an elementary cell oscillate almost out of phase and the center of gravity remains immovable. Therefore, in this case the crystal deformation and accordingly the band edge variation, i.e., the interaction energy, will be proportional to the shift of any atom in an elementary cell. Consequently, the interaction operator of the charge carriers with optical lattice oscillations can be presented as [27]

$$\hat{\mathcal{H}}'_{\mathrm{o}} = \sum_{j=4}^{3s} \boldsymbol{A}_j \boldsymbol{u}_j \tag{5.20}$$

where $\boldsymbol{u}_j$ is the shift corresponding to the j^{th} branch and $\boldsymbol{A}_j$ is a constant vector that is governed by the symmetry of arrangement of the charge carrier energy band minima.

For simplicity, let us consider the scattering of charge carriers as occurring at a specified minimum on one optical branch, and present the vector $\boldsymbol{A}$ in the form

$$\boldsymbol{A} = E_{\text{o}}\boldsymbol{b}_g \tag{5.21}$$

where $\boldsymbol{b}_g = (\pi/a)\boldsymbol{g}$ is the reciprocal lattice vector, $\boldsymbol{g}$ is a unit vector directed from the Brillouin zone center towards the considered minimum and E_{o} is the optical deformation potential constant with dimensions of energy. As in the case of scattering by acoustic phonons, the introduction of a deformation potential constant allows us to characterize to influence of this scattering mechanism.

In this work the phonon dispersion relation was not taken into account and we made the assumption that at $q \to 0$

$$\omega(q) = \omega_0 \tag{5.22}$$

If we also make the assumption that at the considered temperature $k_BT \gg \hbar\omega_0$, it is then possible to neglect the nonelasticity and the following simple expression for the relaxation time for an arbitrary isotropic band can be found (see Ref. [27] for detailed derivation)

$$\tau_{\text{o}}(k,T) = \frac{1}{\pi\hbar}\left(\frac{\hbar\omega_0}{E_{\text{o}}}\right)^2 \frac{\rho a^3}{k_BT}\frac{1}{k^2}\left(\frac{\partial\varepsilon}{\partial k}\right) \tag{5.23}$$

with a the lattice constant of the cubic cell.

Again for simplicity we used a parabolic band structure to obtain an expression for the relaxation time usable in practice. For the parabolic dispersion relation of Eq. (5.18) we obtain

$$\tau_{\text{o}}(\varepsilon,T) = \frac{2}{\pi}\left(\frac{\hbar\omega_0}{E_{\text{o}}}\right)^2 \frac{\hbar^2a^2\rho}{(2m^*k_BT)^{3/2}}\left(\frac{\varepsilon}{k_BT}\right)^{-1/2} \tag{5.24}$$

The temperature and energy dependence of the relaxation time for non-polar optical scattering is thus the same as for scattering by acoustic phonons : $\tau_{\text{a}}(\varepsilon,T) \sim T^{-1}\,\varepsilon^{-1/2}$.

5.4 Polar Optical Phonons Scattering

5.4.1 General Case

In polar crystal like PbTe, optical lattice oscillations produce an electric polarization in addition to the deformation potential. This is due to the fact that optical phonons are a mode of vibration where negative and positive ions oscillate out-of-phase, generating an electrical dipole moment varying with time (hence the name *optical* phonons). Long-wave optical oscillations cause ions of different signs to be shifted towards opposite sides, leading to the lattice polarization. Such polarization propagates in the crystal and forms a polarization wave. This wave causes additional interactions of these optical phonons with charge carriers.

Again for our range of temperature $k_BT \gg \hbar\omega_0$ and we can neglect the nonelasticity. From this and again following the work of B.M. Askerov (Ref. [27]) we obtain for the transition probability

$$W^{\text{po}}_{\boldsymbol{k}\boldsymbol{k}'} = \frac{8\pi^2e^2}{V\epsilon^*}\frac{k_BT}{\hbar}\frac{1}{(\boldsymbol{k}'-\boldsymbol{k})^2}\delta(\varepsilon_{\boldsymbol{k}'}-\varepsilon_{\boldsymbol{k}}) \tag{5.25}$$

where V is the volume and

$$\epsilon^* = \left(\frac{1}{\epsilon_\infty}-\frac{1}{\epsilon_0}\right)^{-1} \tag{5.26}$$

ϵ_∞ and ϵ_0 being respectively the high frequency and static dielectric constant of the crystal.

Substituting this expression in Eq. (5.11), performing the integration over $d\boldsymbol{k}'$ in spherical coordinates with the polar axis along $\boldsymbol{k}$ and using a δ-function in the integral over $\boldsymbol{k}'$ we obtain for an arbitrary isotropic band

$$\tau_{\mathrm{po}}(k,T) = \frac{\epsilon^* \hbar}{2e^2 k_B T} \left(\frac{\partial \varepsilon}{\partial k}\right) \tag{5.27}$$

It can be seen that unlike for non polar optical phonons, $\tau(k)$ does not depend on the phonon frequency. Again for a parabolic dispersion relation of Eq. (5.18) we obtain the expression of the relaxation time for scattering by polar optical phonons

$$\tau_{\mathrm{po}}(\varepsilon,T) = \frac{\hbar^2 \epsilon^*}{e^2 (2m^* k_B T)^{1/2}} \left(\frac{\varepsilon}{k_B T}\right)^{1/2} \tag{5.28}$$

For this type of scattering the energy dependence is then different : $\tau_{\mathrm{po}}(\varepsilon,T) \sim T^{-1}\,\varepsilon^{1/2}$ meaning that the influence of the scattering by polar optical phonons decreases at high energies, as expected [30].

5.4.2 Inclusion of Screening by Charge Carriers

In the previous section we did not include electric potential screening by charge carriers themselves for their interaction with polar optical phonons. As shown in the next chapter, this leads to an overestimation of the scattering due to polar optical phonons and thus a too small conductivity. The screening of Coulomb potential of ions by charge carriers can be included by adding a decreasing exponential to the ion potential [33]

$$\varphi(r) = \frac{q}{4\pi\epsilon\, r} \exp\left(\frac{-r}{r_0}\right) \tag{5.29}$$

with q the electron charge e times the number of protons in the nucleus minus the number of core electrons and r_0 called the radius of the ion field screening. The exponential has the effect of reducing considerably the electric potential when the distance to the ion r increases. This screening causes a renormalization of the longitudinal optical oscillation frequencies

$$\omega^{\mathrm{scr}}(q) = \omega(q) \left(\frac{1 + \frac{\epsilon_\infty}{\epsilon_0}(qr_0)^{-2}}{1 + (qr_0)^{-2}}\right)^{1/2} \tag{5.30}$$

as well as a variation of the interaction energy with polar optical phonons

$$\hat{\mathcal{H}}'_{\mathrm{po\ scr}} = \left(1 + \frac{1}{q^2 r_0^2}\right)^{-1} \hat{\mathcal{H}}'_{\mathrm{po}} \tag{5.31}$$

where $\hat{\mathcal{H}}'_{\mathrm{po}}$ is the Hamiltonian of the interaction if screening was absent. For the limiting frequency of optical phonons at $q \to 0$ it follows that

$$\omega_0^{\mathrm{scr}} = \left(\frac{\epsilon_\infty}{\epsilon_0}\right)^{1/2} \omega_0 \tag{5.32}$$

The radius of ion field screening r_0 is defined by

$$r_0^{-2} = \frac{4\pi e^2}{\epsilon} \int -\frac{\partial f_0}{\partial \varepsilon}\, g(\varepsilon)\, d\varepsilon \tag{5.33}$$

with $g(\varepsilon)$ the density of states [33].

Taking into account that

$$-\frac{\partial f_0}{\partial \varepsilon} = \frac{1}{k_B T} f_0(1 - f_0) \tag{5.34}$$

leads to [27]

$$\int -\frac{\partial f_0}{\partial \varepsilon} g(\varepsilon)\, d\varepsilon \simeq \frac{n}{k_B T} \tag{5.35}$$

By injecting this result in Eq. (5.33), it is easy to obtain for the screening radius

$$r_0 = \left(\frac{\epsilon\, k_B T}{4\pi e^2 n}\right)^{1/2} \tag{5.36}$$

The relaxation time for scattering by polar optical phonons is then multiplied by a screening factor $1/F_{\text{po}}(k)$:

$$\tau_{\text{po scr}}(k, T) = \frac{\epsilon^* \hbar}{2e^2 k_B T} \frac{1}{F_{\text{po}}(k)} \left(\frac{\partial \varepsilon}{\partial k}\right) \tag{5.37}$$

where

$$F_{\text{po}}(k) = 1 - \frac{2}{\delta} \ln(\delta + 1) + \frac{1}{\delta + 1} \tag{5.38}$$

with $\delta = (2kr_0)^2$.

The relaxation time for polar scattering by screened optical phonons in case of a parabolic model (Eq. (5.18)) is thus given by

$$\tau_{\text{po scr}}(\varepsilon, T) = \frac{\hbar^2 \epsilon^*}{e^2 (2 m_{d0} k_B T)^{1/2}} \frac{1}{F_{\text{po}}(\varepsilon)} \left(\frac{\varepsilon}{k_B T}\right)^{1/2} \tag{5.39}$$

Figure (5.1) shows the energy and temperature dependence of the function F_{po} for a doping level $n = 5 \times 10^{19}$ cm^{-3} (n appearing in the expression of r_0 Eq. (5.36)). As expected the inclusion of screening reduces considerably the influence of this type of scattering, the relaxation time is multiplied by a factor varying from 5 to 50 in our range of temperature and energy. As T and ε increase, F_{po} becomes greater and thus screening becomes less important. However in the temperature and energy range of interest, this still makes a very significant difference on the total relaxation time.

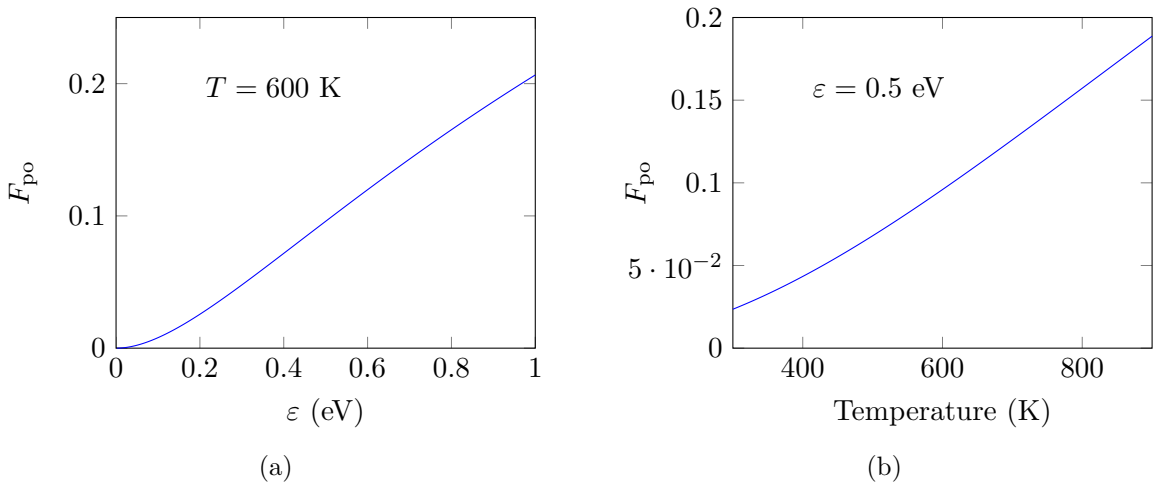

Figure 5.1: Energy and temperature dependence of the F_{po} screening factor. (a) Energy dependence ($T = 600$ K). (b) Temperature dependence ($\varepsilon = 0.5$ eV).

5.5 Comparison of Each Mechanism and Resulting Relaxation Time

In this section we calculated the relaxation time for the three different scattering mechanisms (with and without screening for polar optical phonons scattering) and the total relaxation time resulting of each contribution from Eqs. (5.19), (5.24), (5.28) and (5.39). The material parameters appearing in these equations were taken from reference [34] and are given in Table 5.1. These parameters are given at 300 K and we assumed in this work that they remain constant at other temperatures (except for the effective mass, see below). Therefore the temperature dependence of the relaxation times comes only from the explicit presence of T in Eqs (5.19), (5.24), (5.28) and (5.39) and from the T dependence of the effective mass.

In the literature, the experimental effective mass for PbTe is always given by two distinct components m_t and m_l corresponding to the transverse and longitudinal effective masses. This comes from the fact that the band structure of lead telluride is anisotropic and the dispersion relation is often approximated by

$$\varepsilon = \frac{\hbar^2}{2}\left(\frac{2k_t^2}{m_t} + \frac{k_l^2}{m_l}\right) \tag{5.40}$$

where k_t and k_l are the magnitude of the transverse and longitudinal components of $\boldsymbol{k}$.

In order to convert this model to an isotropic parabolic model, we can make the following changes of variables [30]

$$k_t'^2 = \left(\frac{m_l}{m_t}\right)^{1/3} k_t^2 \tag{5.41}$$

and

$$k_l'^2 = \left(\frac{m_t}{m_l}\right)^{2/3} k_l^2 \tag{5.42}$$

which gives for the energy dispersion

$$\varepsilon = \frac{\hbar^2}{2}\left(\frac{2k_t'^2}{(m_t^2 m_l)^{1/3}} + \frac{k_l^2}{(m_t^2 m_l)^{1/3}}\right) \tag{5.43}$$

If we define a *density of states effective mass* $m_d = (m_t^2 m_l)^{1/3}$ we obtain

$$\varepsilon = \frac{\hbar^2}{2m_d}\left(2k_t'^2 + k_l'^2\right) = \frac{\hbar^2 k'^2}{2m_d} \tag{5.44}$$

As said before it is found experimentally that the density of states effective mass is temperature-dependent. This comes from the T dependence of the transverse effective mass m_t. The experimental values taken from [30] are

$$m_l = 0.24\, m_0 \tag{5.45}$$

$$m_t = 0.02459 + (8.659341 \times 10^{-5})T\, m_0 \tag{5.46}$$

This temperature-dependent experimental effective mass is incorporated in our parabolic model of Eq. (5.18) and replace m^* in order to calculate $\tau(\varepsilon, T)$. The three equations for the relaxation times then become

$$\tau_{\mathrm{a}}(\varepsilon,T)=\frac{2\pi\hbar^4\rho v_0^2}{E_{\mathrm{a}}^2(2m_d(T)k_BT)^{3/2}}\left(\frac{\varepsilon}{k_BT}\right)^{-1/2} \tag{5.47}$$

$$\tau_{\mathrm{o}}(\varepsilon,T)=\frac{2}{\pi}\left(\frac{\hbar\omega_0}{E_{\mathrm{o}}}\right)^2\frac{\hbar^2a^2\rho}{(2m_d(T)k_BT)^{3/2}}\left(\frac{\varepsilon}{k_BT}\right)^{-1/2} \tag{5.48}$$

$$\tau_{\mathrm{po}}(\varepsilon,T)=\frac{\hbar^2\epsilon^*}{e^2(2m_d(T)k_BT)^{1/2}}\frac{1}{F_{\mathrm{scr}}(\varepsilon)}\left(\frac{\varepsilon}{k_BT}\right)^{1/2} \tag{5.49}$$

with F_{scr} equals to 1 in case of no screening and equals to F_{po} (Eq. (5.38)) if screening is taken into account.

Figures 5.2 and 5.3 present the energy and temperature dependence of the inverse of the different relaxation times calculated from these equations with the parameters of Table 5.1. The inverses of the relaxation times are useful quantities in order to compare the influence of the different scattering mechanisms. Indeed according to Eq. (5.2) the inverse of the total relaxation time is obtained simply by summing the contributions of each mechanism and it allows us to compare easily the relative influence of each of them. Figure 5.2 presents the results without screening and Figure 5.3, the results when screening is included. It is important to notice that the screening plays a role only in the polar optical scattering and consequently only the blue and purple curves, corresponding to τ_{po} and τ_{tot} are different in the two figures. The red and green curves corresponding respectively to to τ_{a} and τ_{o} are the same in both graphs but with different scaling. As expected the three scattering mechanisms become more effective when temperature increases, resulting in a smaller τ. It can also be seen that when the screening is not taken into account, polar scattering by optical phonons is the dominant mechanism at every energy but that its influence is considerably reduced when screening is included. As shown in the next chapter the transport coefficients are in better agreement with experimental datas when screening is taken into account.

However, the inclusion of screening as made in Eq. (5.39) changes completely the energy dependence of τ_{po}. The influence of this type of scattering is no longer reduced when energy increases (see Figure 5.3). This should not be the case, the screening should just lower the global influence of this scattering mechanism without affecting the energy and temperature dependence.

The next paragraphs explain how screening was taken into account without changing the shape of the energy and temperature curves, namely respecting the condition of reduced influence of this type of scattering at high energies.

In order to better approximate the influence of polar scattering by optical phonons, we also used the theoretical calculation of $\tau_{\mathrm{po\ scr}}(\varepsilon,T)$ for PbTe made by Ahmad & Mahanti [30]. In their work the non-parabolic Kane model for energy dispersion was used. They included screening in this framework and they used the same parameters as we did (Table 5.1) for the calculation of $\tau_{\mathrm{po}}(\varepsilon,T)$. They also included the temperature-dependent effective mass of Eqs. (5.45 and (5.46).

The data we used are values of the relaxation time for polar optical scattering at 3 temperatures : 300, 600 and 900 K and 4 energies : 0.02, 0.1, 0.2 and 0.3 eV for a total of 12 relaxation times. In order to have an analytical expression for τ_{po} to give to BoltzTraP, we fitted these data with power law functions for energy and temperature.

First we showed that the energy and temperature dependence can be assumed to be independent of each other by scaling the curves of energy dependence at different temperatures to one temperature (300 K) and the curves of temperature dependence at different energies to one energy (0.3 eV) and by comparing them. For the energy dependence this is made by scaling the points at 0.3 eV and 600 and 900 K to the point at 0.3 eV and 300 K and multiplying the relaxation time at other energies by the same scaling factors. A similar method is used for the

Table 5.1: Parameters used to calculate the relaxation times for different scattering mechanisms (Refs. [34] and [30]).

Parameter	Unit of measurement	Value
m_l	m_0	0.24
m_t	m_0	$0.02459 + (8.659341 \times 10^{-5})T$
ρv_0^2	$\mathrm{N\,m^{-2}}$	0.71×10^{11}
E_a	eV	15
$\hbar\omega_0$	eV	0.0136
E_o	eV	26
ρ	$\mathrm{g\,cm^{-3}}$	8.24
a	Å	6.34
ϵ_0	ϵ_vacuum	400
ϵ_∞	ϵ_vacuum	32.6

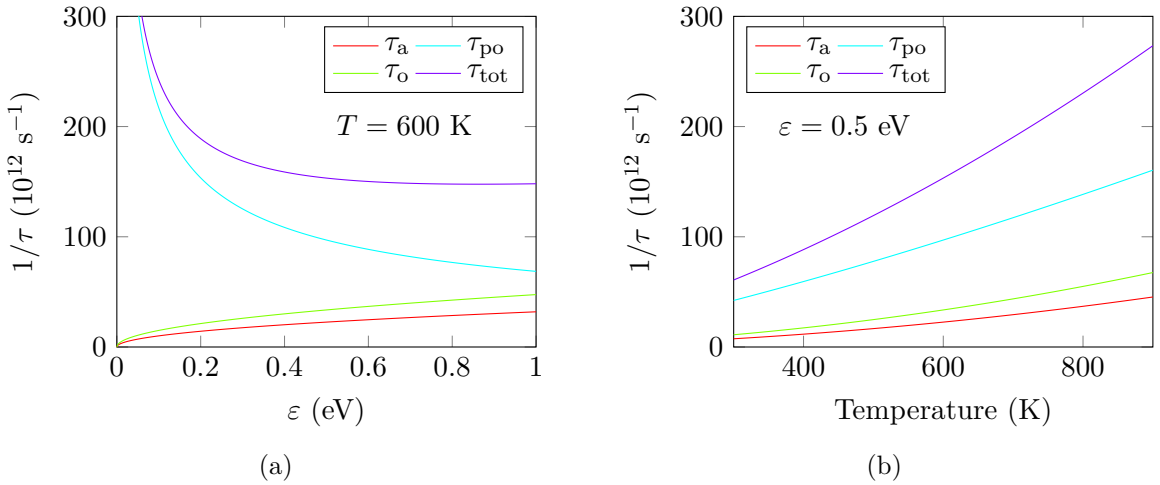

Figure 5.2: Energy and temperature dependence of the inverse of the relaxation time of the three dominant scattering mechanisms (τ_a, τ_o and τ_{po}) and the total resultant of them τ_{tot} in PbTe according to the parabolic model without screening for polar optical scattering. (a) Energy dependence ($T = 600$ K). (b) Temperature dependence ($\varepsilon = 0.5$ eV).

temperature dependence. Figure (5.4) presents the scaled curves and it can be seen that the obtained relaxation times are almost the same, justifying the assumption. Knowing this, the equation for the relaxation can be expressed as

$$\tau^{\mathrm{fit}}_{\mathrm{po\ scr}}(\varepsilon, T) = F_1(\varepsilon)\, F_2(T) = a\, \varepsilon^r\, T^{-p} \tag{5.50}$$

To find $F_1(\varepsilon)$ we fitted the relaxation times at 300 K with a least squared method implemented in MATLAB. We then used the same method to fit the temperature dependence $F_2(T)$. The results and the obtained expression for F_1 and F_2 are presented on Figure (5.5). The exponent for the energy dependence is found to be $r = 0.19$ in accordance with the the fact that the relaxation time for scattering by polar optical phonons must increase when energy increases but still much lower than the $r = 1/2$ exponent found when no screening is considered.

Now that we have an analytical expression for $\tau^{\mathrm{fit}}_{\mathrm{po\ scr}}$ it is possible to obtain the $F^{\mathrm{fit}}_{\mathrm{po}}$ in this case and compare it to F_{po} obtained with the theory of screening. We have the relation

$$\tau^{\mathrm{fit}}_{\mathrm{po\ scr}} = \frac{1}{F^{\mathrm{fit}}_{\mathrm{po}}} \tau_{\mathrm{po}} \tag{5.51}$$

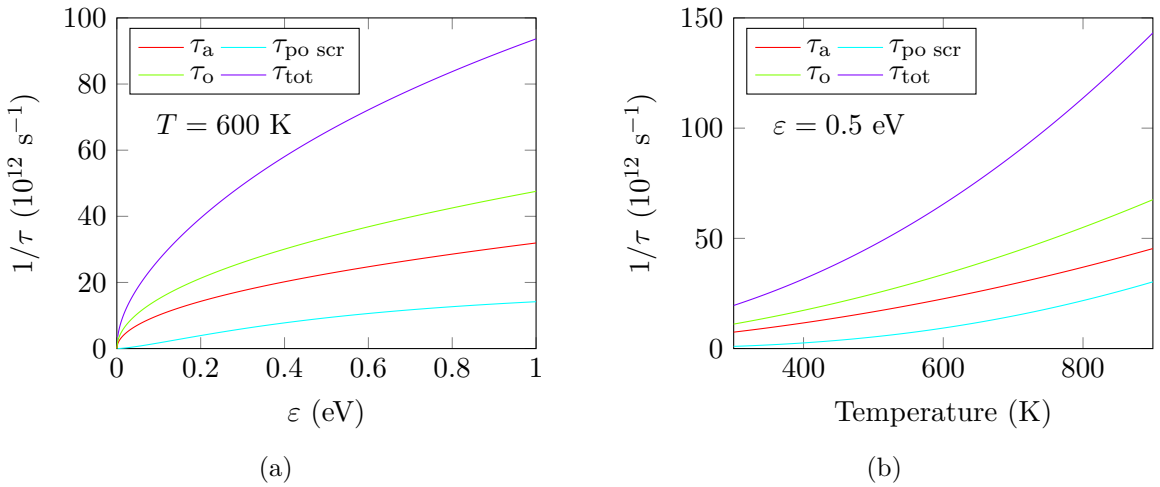

(a) (b)

Figure 5.3: Energy and temperature dependence of the inverse of the relaxation times of the three dominant scattering mechanisms (τ_a, τ_o and $\tau_{po\ scr}$) and the total resultant of them τ_{tot} in PbTe according to the parabolic model with screening for polar optical scattering. (a) Energy dependence ($T = 600$ K). (b) Temperature dependence ($\varepsilon = 0.5$ eV).

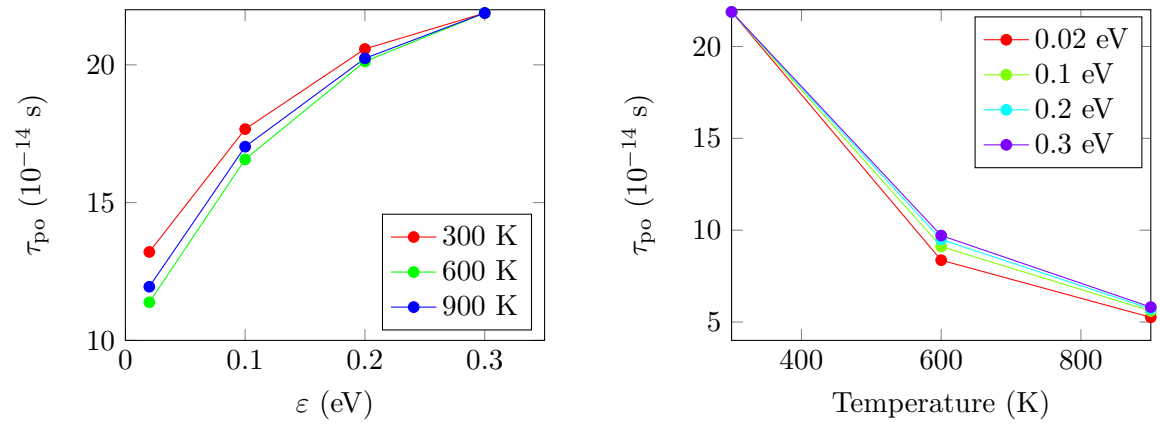

(a) (b)

Figure 5.4: Energy and temperature dependence of the scaled relaxation times for polar scattering by optical phonons τ_{po} calculated by Ahmad & Mahanti [30]. (a) Energy dependence (scaled to $T = 300$ K). (b) Temperature dependence (scaled to $\varepsilon = 0.3$ eV).

where τ_{po} is the relaxation time when screening is not included. F_{po}^{fit} is the simply given by

$$F_{po}^{fit} = \frac{\tau_{po}}{\tau_{po\ scr}^{fit}} \tag{5.52}$$

The graphs of this comparison are presented on Figure 5.6. It can be seen that in both case the influence of screening is reduced when energy is increased but that it remains almost constant with temperature when screening is included through a fitted model. Obviously, when no screening is included, F_{po} is simply equals to 1.

Let us now compare the influence of polar optical scattering according to the 3 tested models, namely without screening, with theoretical inclusion of screening and with the fitted model including screening. Figure 5.7 presents the plots of the inverse of the relaxation times for the 3 models. It is seen that the third one is in accordance with what we expected : a reduced influence of this mechanism but with the same energy and temperature dependence as in the general case without screening.

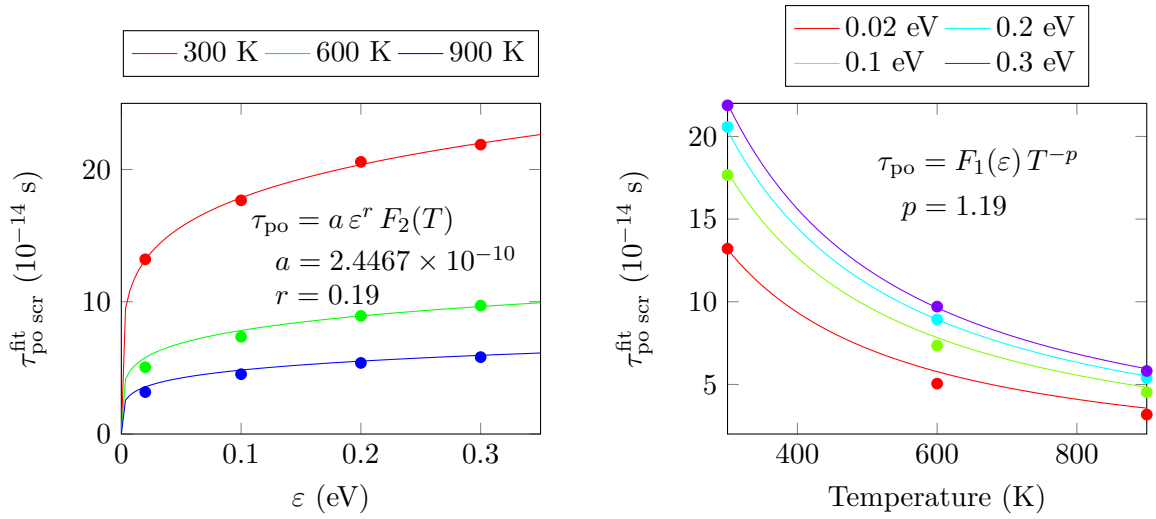

(a) (b)

Figure 5.5: Fits of the energy and temperature dependence of the relaxation time for polar scattering by optical phonons $\tau^{\text{fit}}_{\text{po scr}}$. The dots represents the values from Ref. [30] and the solid lines are the obtained fits. (a) Energy dependence (Fit on the $T = 300$ K values). (b) Temperature dependence (Fit on the $\varepsilon = 0.3$ eV values). The final expression is $\tau^{\text{fit}}_{\text{po scr}} = a\,\varepsilon^r\,T^{-p}$.

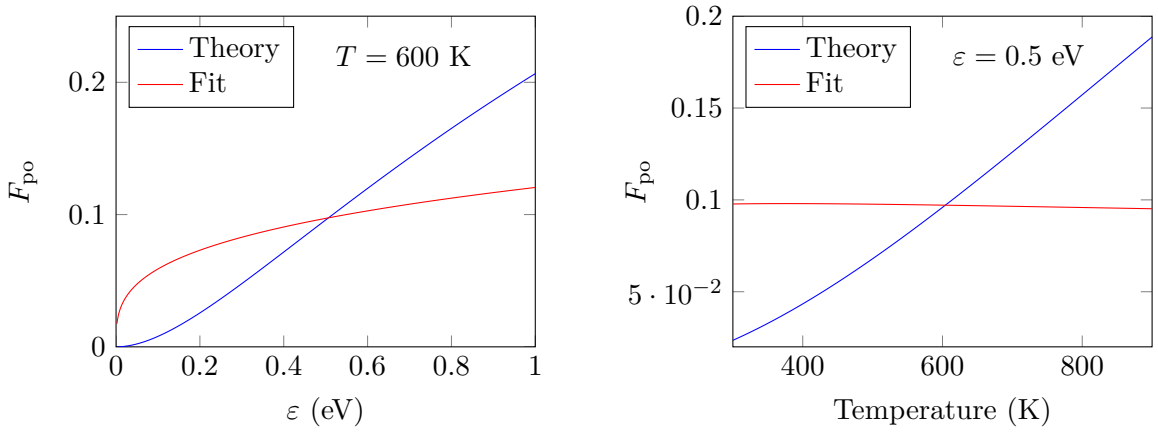

(a) (b)

Figure 5.6: Comparison between F_{po} for the theoretical inclusion screening and $F^{\text{fit}}_{\text{po}}$ resulting from the fit. (a) Energy dependence ($T = 600$ K). (b) Temperature dependence ($\varepsilon = 0.5$ eV).

Figure (5.8) shows the influence of the different scattering mechanisms when this last model is used : $\tau^{\text{fit}}_{\text{po scr}}$ (Eq. (5.50)). In this case, the three scattering mechanisms are of the same order of magnitude. The next section explains how we implemented all these models in the BoltzTraP code.

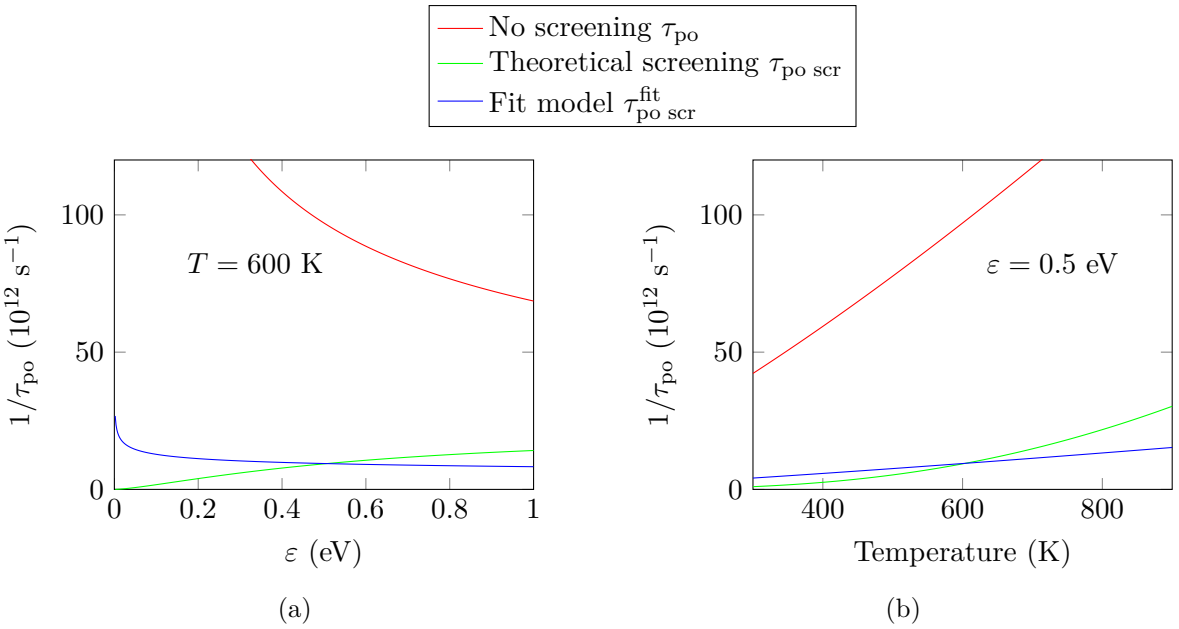

Figure 5.7: Comparison of the inverse of the relaxation for polar optical scattering for the 3 different models. (a) Energy dependence ($T = 600$ K). (b) Temperature dependence ($\varepsilon = 0.5$ eV).

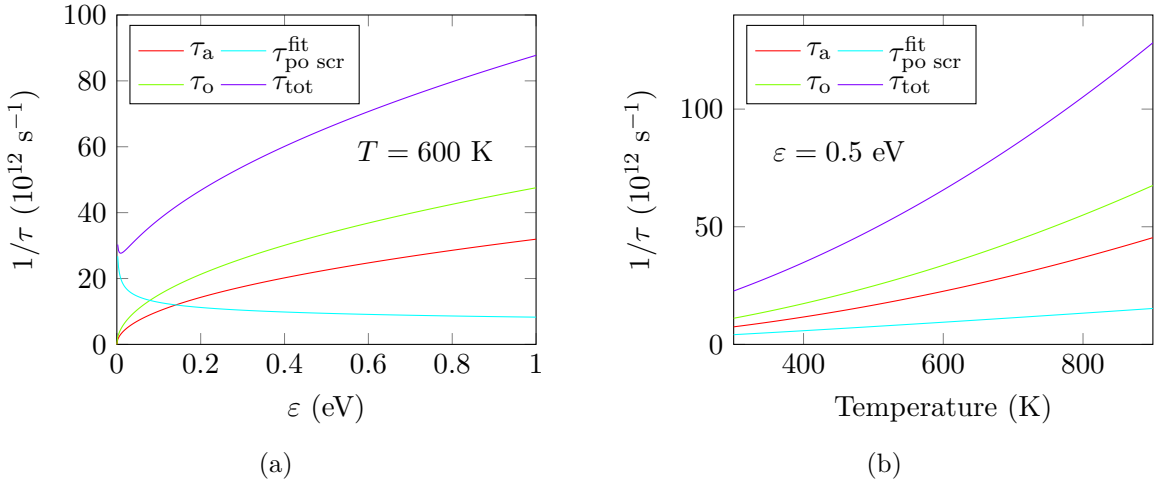

Figure 5.8: Energy and temperature dependence of the inverse of the relaxation times of the three dominant scattering mechanisms (τ_{a}, τ_{o} and $\tau^{\text{fit}}_{\text{po scr}}$) and the total resultant of them τ_{tot} in PbTe according to the parabolic model. (a) Energy dependence ($T = 600$ K). (b) Temperature dependence ($\varepsilon = 0.5$ eV).

5.6 Implementation of Varying Relaxation Times in BoltzTraP

In order to use these models in BoltzTraP, we modified the code of the program in the subroutine FERMIINTEGRALS. The three Eqs (5.47), (5.48) and (5.49) can be expressed in the form

$$\tau(\varepsilon, T) = \tau_0(\varepsilon_0, T_0) \left(\frac{m_d(T)}{m_d(T_0)}\right)^{r-3/2} \left(\frac{T}{T_0}\right)^{s} \left(\frac{\varepsilon}{\varepsilon_0}\right)^{r-1/2} \tag{5.53}$$

where the five parameters τ_0, ε_0, T_0, s and r are input parameters depending of the scattering mechanism. The different input values used in this work are summarized in Table 5.2, as said before the material parameters used for the calculation of τ_0 are listed in Table 5.1.

In order to add the screening for polar optical scattering, we add the calculation of $F_{\text{po}}(\varepsilon)$ in the code from Eq. (5.1) and we divided τ_{po} by it in case of the theoretical model. For the fitted model, we simply used the analytical expression of Eq. (5.50) since screening is already included in it.

To compute the total relaxation time when each mechanism is taken into account, we modified the program so that it can take 15 input arguments (five for each mechanisms). The three relaxation times are then calculated separately and summed accordingly to the Matthiessen law of Eq. (5.2). The corrections and modifications made to the program in order to use energy and temperature dependent $\tau(\varepsilon, T)$ can be found in appendix C.

Table 5.2: Input parameters to give to BoltzTraP for each scattering mechanism.

Type of scattering	r	s	$\tau_0(\varepsilon_0, T_0)$
Acoustic phonons	0	-1	$\frac{2\pi\hbar^4\rho v_0^2\,\varepsilon_0^{-1/2}}{E_{\text{a}}^2\,k_B T(2m_d(T_0))^{3/2}}$
Optical phonons	0	-1	$\frac{2(\hbar\omega_0)^2\,\hbar^2 a^2\rho\,\varepsilon_0^{-1/2}}{\pi\,E_{\text{o}}^2 k_B T_0(2m_d(T_0))^{3/2}}$
Polar optical phonons	1	-1	$\frac{\hbar^2\epsilon^*\,\varepsilon_0^{1/2}}{e^2 k_B T_0(2m_d(T_0))^{1/2}}$

Chapter 6

Transport Coefficients of PbTe with Different Relaxation Time Models

Contents

In this chapter the temperature dependence of the transport properties of PbTe is computed by solving the Boltzmann Transport Equation in the Relaxation Time Approximation using the BoltzTraP program. The relaxation times corresponding to the different scattering mechanisms derived in Chapter 5 are tested both separately and all together in order to point out the relative influence of each of them. The calculations are also performed at different carriers concentration to check the effect of doping on the thermoelectric properties of PbTe. Finally in the last section a comparison between our results and some experimental data found in the literature is realised.

6.1 Seebeck Coefficient

In Chapter 4 we showed that the Seebeck coefficient under zero electrical current can be calculated in the framework of the Boltzmann transport by the equation

$$S = L_{11}^{-1} L_{12} \tag{6.1}$$

with the integrals L_{11} and L_{12} defined in Eqs. (4.42) and (4.43) and rewritten here for simplicity

$$L_{11}^{\alpha\beta} = \frac{e^2}{4\pi^3\hbar} \int d\varepsilon\, \tau(\varepsilon) \left(-\frac{\partial f_0}{\partial \varepsilon}\right) \int d\Omega_\varepsilon \frac{v^\alpha v^\beta}{|\boldsymbol{v}|} \tag{6.2}$$

$$L_{12}^{\alpha\beta} = -\frac{e}{4\pi^3\hbar\, T} \int d\varepsilon\, \tau(\varepsilon)(\varepsilon - \mu) \left(-\frac{\partial f_0}{\partial \varepsilon}\right) \int d\Omega_\varepsilon \frac{v^\alpha v^\beta}{|\boldsymbol{v}|} \tag{6.3}$$

In both of these equations the relaxation time $\tau(\varepsilon)$ appears in the integral over the energy. In case of a constant relaxation time, τ does not depend on energy and can thus be taken outside the integral. Consequently, τ appears on both the numerator and denominator of Eq. (6.1) and it simplifies. This explains why there is no need to define a relaxation time in BoltzTraP to obtain a good estimation of the Seebeck coefficient. When an energy and temperature dependent τ is used, $\tau(\varepsilon, T)$ remains in the integral and no simplifications are possible.

The temperature dependence of the Seebeck coefficient for n- and p-type PbTe at a fixed doping level of 5×10^{19} charge carriers per cm^3 is presented on Figure 6.1. The results of the three different models for the screening in polar optical scattering derived in the previous chapter are presented. It can be seen that even with an energy and temperature dependent τ, S does not differ significantly from the case where a constant τ is used and that the addition of screening is not of great influence on the resulting Seebeck coefficient. Consequently we can say that the use of a constant relaxation time is a sufficiently good approximation for the estimation of the Seebeck coefficient of thermoelectric materials.

Figure 6.2 presents the temperature dependence of S for n- and p-type PbTe at different doping levels when the total relaxation time taking the three types of phonon scattering into account is used, with again a comparison of the three models for screening. It can be seen, as one would expect, that the maximum of the absolute value of S, that corresponds to the Fermi level position close to a band edge, moves to higher temperatures for higher doping levels in both n- and p-type material but that this maximum also decreases with the augmentation of carriers. This is a normal behaviour since the more a semiconductor is doped the more it will exhibit the properties of a metal which are not good thermolectric materials and have a small S. However when temperature raises, $|S|$ for high doping levels increases while it yields zero for low doping levels. At last it can be seen that the inclusion of screening does not bring significant changes to the results, what is not surprising since we saw that the energy and temperature dependence of the relaxation time does not play an important role in the estimation of S.

6.2 Electrical Conductivity

Again in Chapter 4 it was shown that the electrical conductivity can be calculated by the equation

$$\sigma = L_{11} \tag{6.4}$$

with the integral L_{11} defined in Eq. (4.42).

In this case the term $\tau(\varepsilon)$ appears only on the numerator under the integral sign and it thus plays a major role. When a constant τ is used, it can again be taken outside the integral and it acts only as a coefficient. Therefore in case of a constant τ, BoltzTraP outputs the conductivity divided by the relaxation time : σ/τ. In order to obtain the conductivity, one must simply multiply it by the chosen τ. For varying relaxation times taking into account different types of scattering, $\tau(\varepsilon, T)$ stays in the integral and σ is then greatly affected by the temperature and energy dependence of $\tau(\varepsilon, T)$.

Figure 6.3 presents the conductivity for different scattering mechanisms at a fixed doping level as a function of temperature in a log-log axis base, with again a comparison of the three models for screening. First it can be seen that for a constant τ, fixed arbitrary to $\tau = 10^{-14}$ s, the conductivity does almost not depend on temperature while for other scattering models, it decreases exponentially. As shown in the next section, the correct T-dependence is of course a decreasing exponential, since the augmentation of temperature generates more vibrations and consequently more phonons for scattering. The constant relaxation time approximation is then a really bad approximation in the estimation of σ at different temperatures and energy and temperature dependent models give much better shape to the curves. Secondly one can notice that the value of the conductivity at one fixed temperature is greatly affected by the considered scattering mechanism: as expected σ for one type of scattering separately is 2 to 10 times greater than σ when all phonon scattering mechanisms are taken into account. This is of course normal since the more scattering processes are included, the shorter is the total relaxation time and therefore the smaller is the conductivity. Thirdly it is interesting to analyse the effect of screening on the conductivity in case of only polar optical scattering. For both n- and p-type PbTe, the inclusion of screening considerably increases σ, for both the theoretical and fitted model. As mentioned before this is due to the drastic augmentation of τ_{po} when screening was

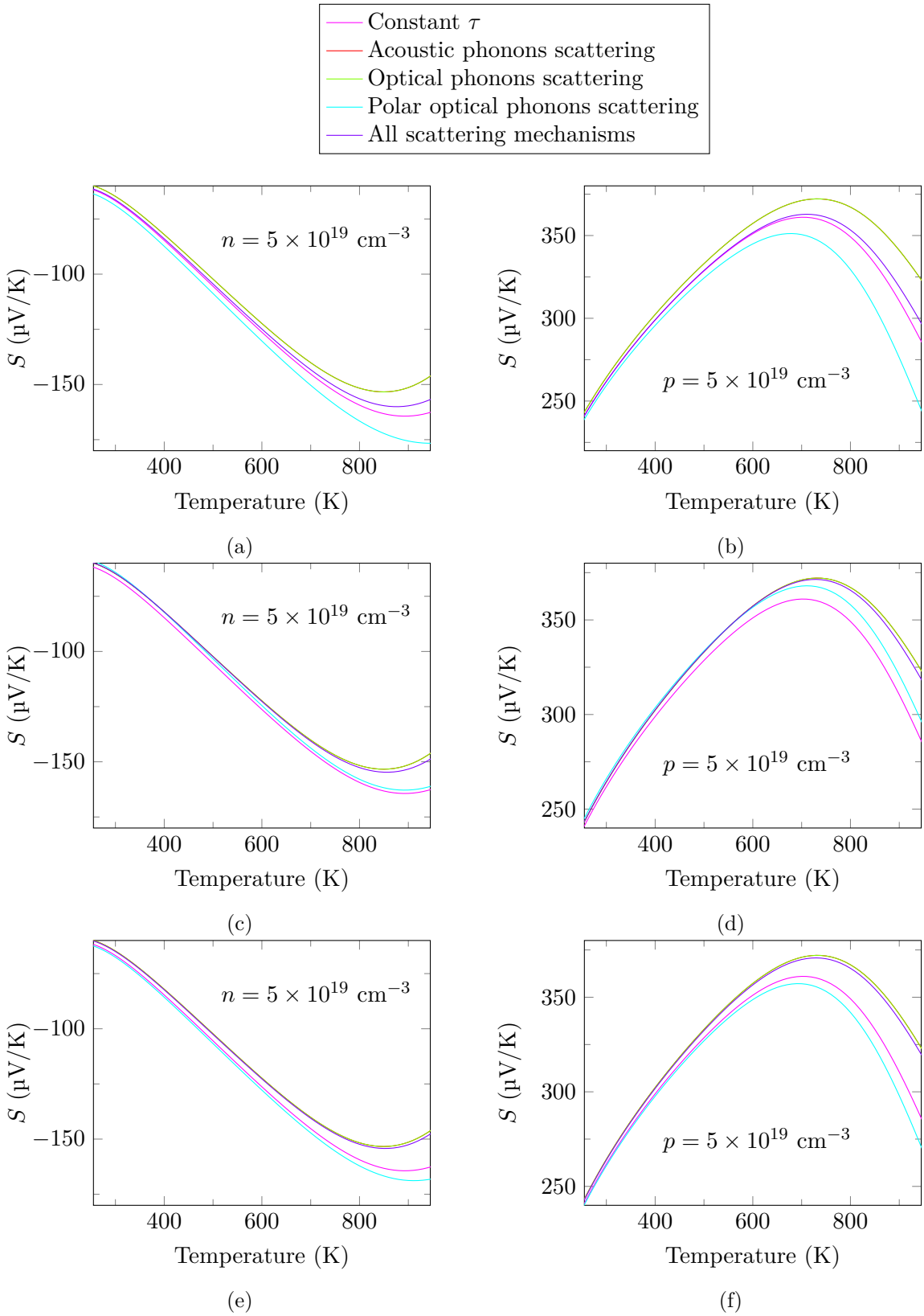

Figure 6.1: Temperature dependence of the Seebeck coefficient for the different scattering mechanisms separately and all together. (a) and (b) : no screening for τ_{po}, (c) and (d) : theoretical screening for τ_{po}, (e) and (f) : fitted model for τ_{po} that includes screening. For comparison, the results obtained with a constant relaxation time of $\tau = 10^{-14}$ s are also represented in pink.

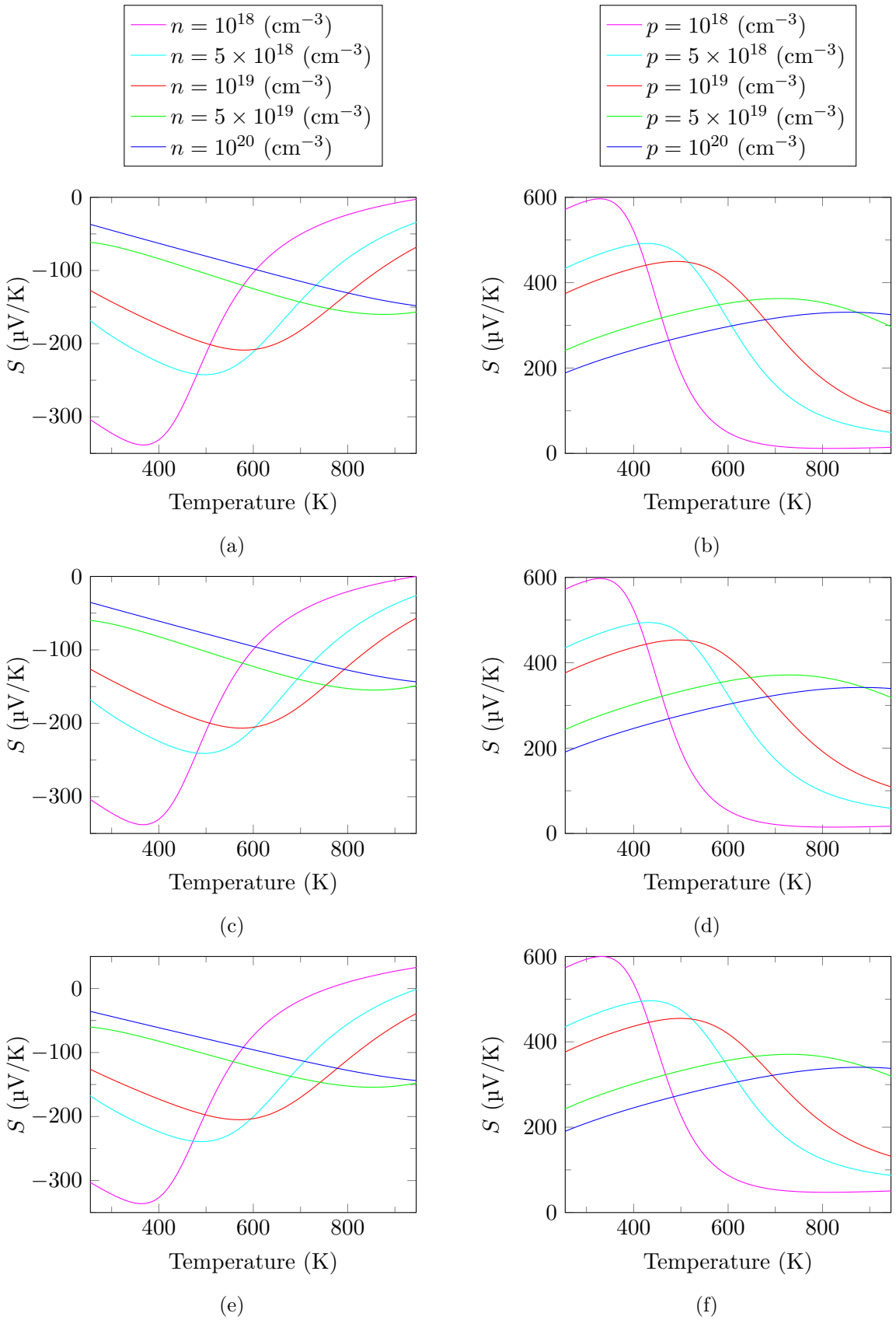

Figure 6.2: Temperature dependence of the Seebeck coefficient at different doping levels computed with a relaxation time taking all phonons scattering mechanisms into account. (a) and (b) : no screening for τ_{po}, (c) and (d) : theoretical screening for τ_{po}, (e) and (f) : fitted model for τ_{po} that includes screening.

included, resulting in much smaller influence of this scattering mechanism. Consequently the total electrical conductivity is also significantly higher with screening than without.

Figure 6.4 presents the temperature dependence of the conductivity of n- and p-type PbTe at different doping levels when the total relaxation is used. As expected the conductivity is much greater for high doping levels simply because more charge carriers are present to conduct electricity. As explained just above, σ decreases when temperature raises due to phonon scattering but for low doping levels, it starts to increases at temperatures around $\sim 400 - 500$ K. This is due to the thermal generation of intrinsic charge carriers in the semiconductor at these temperatures, increasing the conductivity. This effect is not noticeable for higher doping levels because the augmentation of carriers is small in comparison to their total number. The influence of screening leading to an higher conductivity is clearly perceptible on this figure for both n- and p-type PbTe and especially at low temperature and carriers concentration.

6.3 Power Factor

As mentioned in Chapter 2, the efficiency of a thermoelectric material is characterized by its figure of merit

$$z\,T = \frac{\sigma\,S^2\,T}{\kappa_e + \kappa_l} \tag{6.5}$$

where the term $\sigma\,S^2$ in the numerator is called the power factor (PF).

Having the highest power factor possible is thus crucial in order to maximize the thermoelectric properties of a material. From the computed Seebeck coefficient and electrical conductivity presented in the previous sections, we easily obtained the power factor by application of Eq. (6.5).

Figure 6.5 shows the temperature dependence of the PF for different types of scattering at a fixed doping level, with again a comparison of the three models for screening. As expected, the power factor depends greatly of the considered relaxation mechanism, PF being much larger for each type of scattering separately than when calculated with the τ_{tot}. It can also be seen that, without surprises, the power factor calculated with a constant τ gives a totally wrong temperature dependence.

The temperature dependence of the power factor of n- and p-type PbTe at different doping levels when the total relaxation time is used is presented on Figure 6.6. The significant differences in the magnitude of $|S|$ between n- and p-type PbTe leads to consequent differences in the computed power factors (one order of magnitude). In the next section the comparison with experimental data shows that the PF for the p-type is totally overestimated due to an overestimation of both the Seebeck coefficient and the electrical conductivity in p-type PbTe.

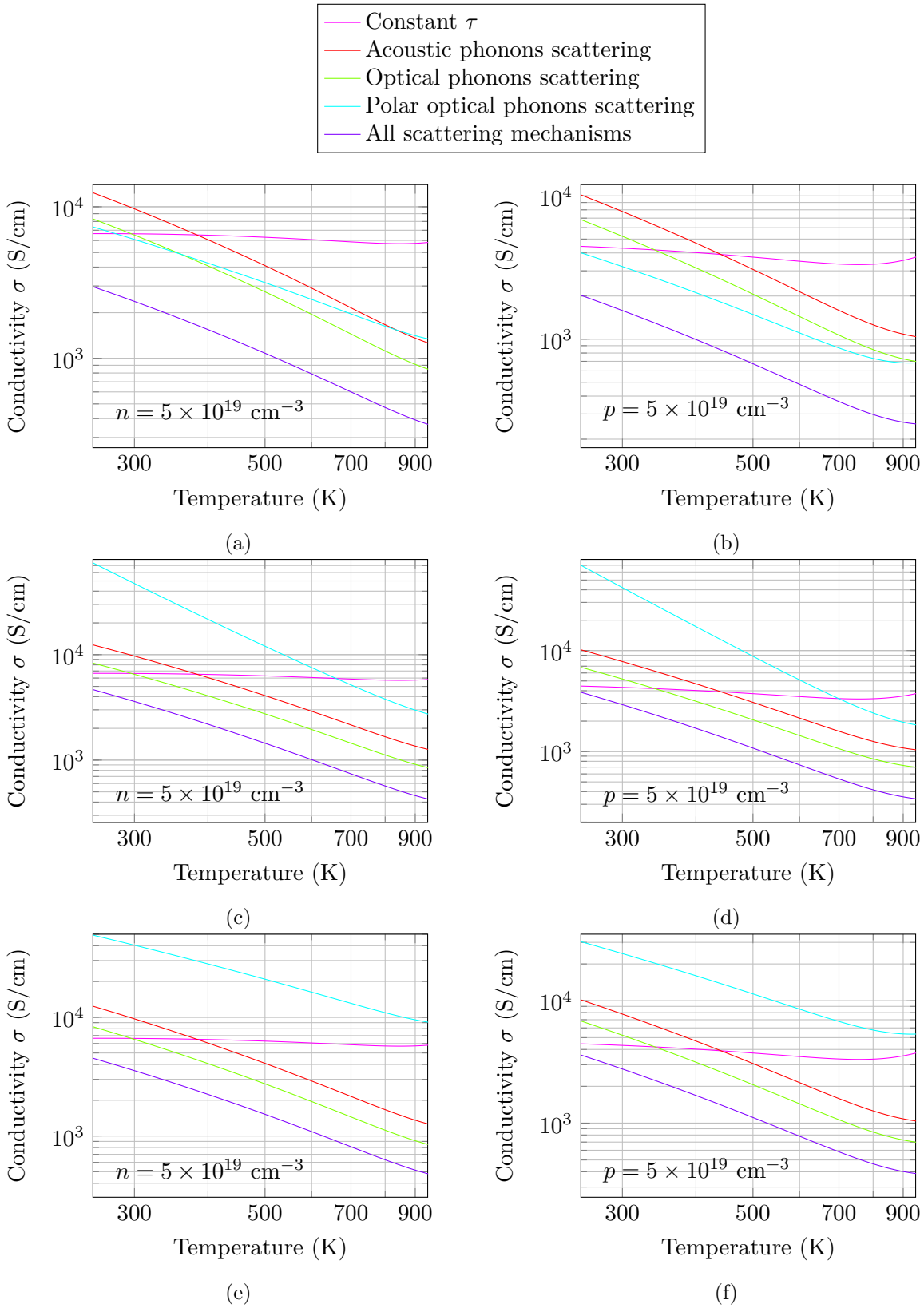

Figure 6.3: Temperature dependence of the electrical conductivity for the different scattering mechanisms separately and all together. (a) and (b) : no screening for τ_{po}, (c) and (d) : theoretical screening for τ_{po}, (e) and (f) : fitted model for τ_{po} that includes screening. For comparison, the results obtained with a constant relaxation time of $\tau = 10^{-14}$ s are also represented in pink.

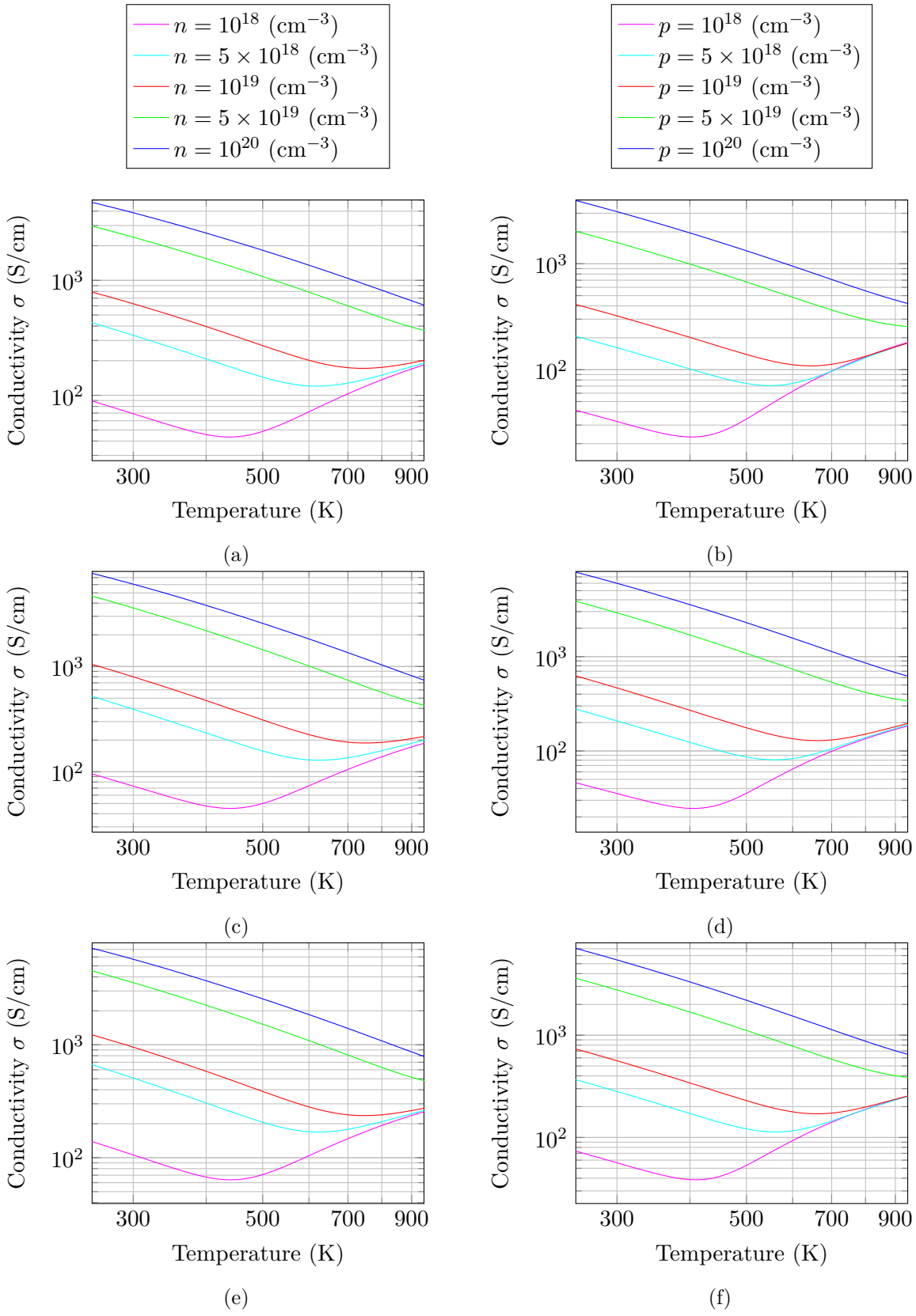

Figure 6.4: Temperature dependence of the Seebeck coefficient at different doping levels computed with a relaxation time taking all phonons scattering mechanisms into account. (a) and (b) : no screening for τ_{po}, (c) and (d) : theoretical screening for τ_{po}, (e) and (f) : fitted model for τ_{po} that includes screening.

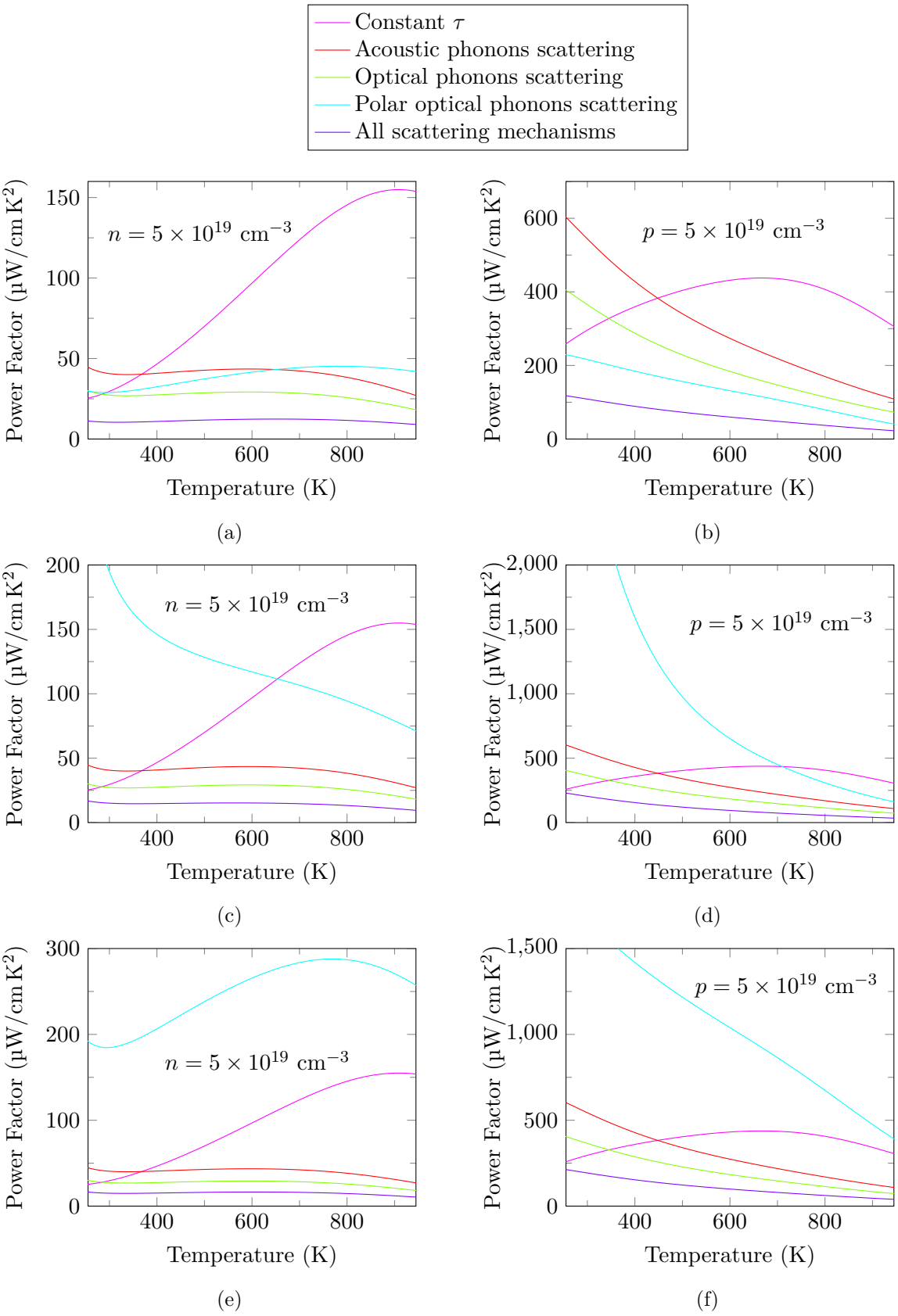

Figure 6.5: Temperature dependence of the power factor for the different scattering mechanisms separately and all together. (a) and (b) : no screening for τ_{po}, (c) and (d) : theoretical screening for τ_{po}, (e) and (f) : fitted model for τ_{po} that includes screening. For comparison, the results obtained with a constant relaxation time of $\tau = 10^{-14}$ s are also represented in pink.

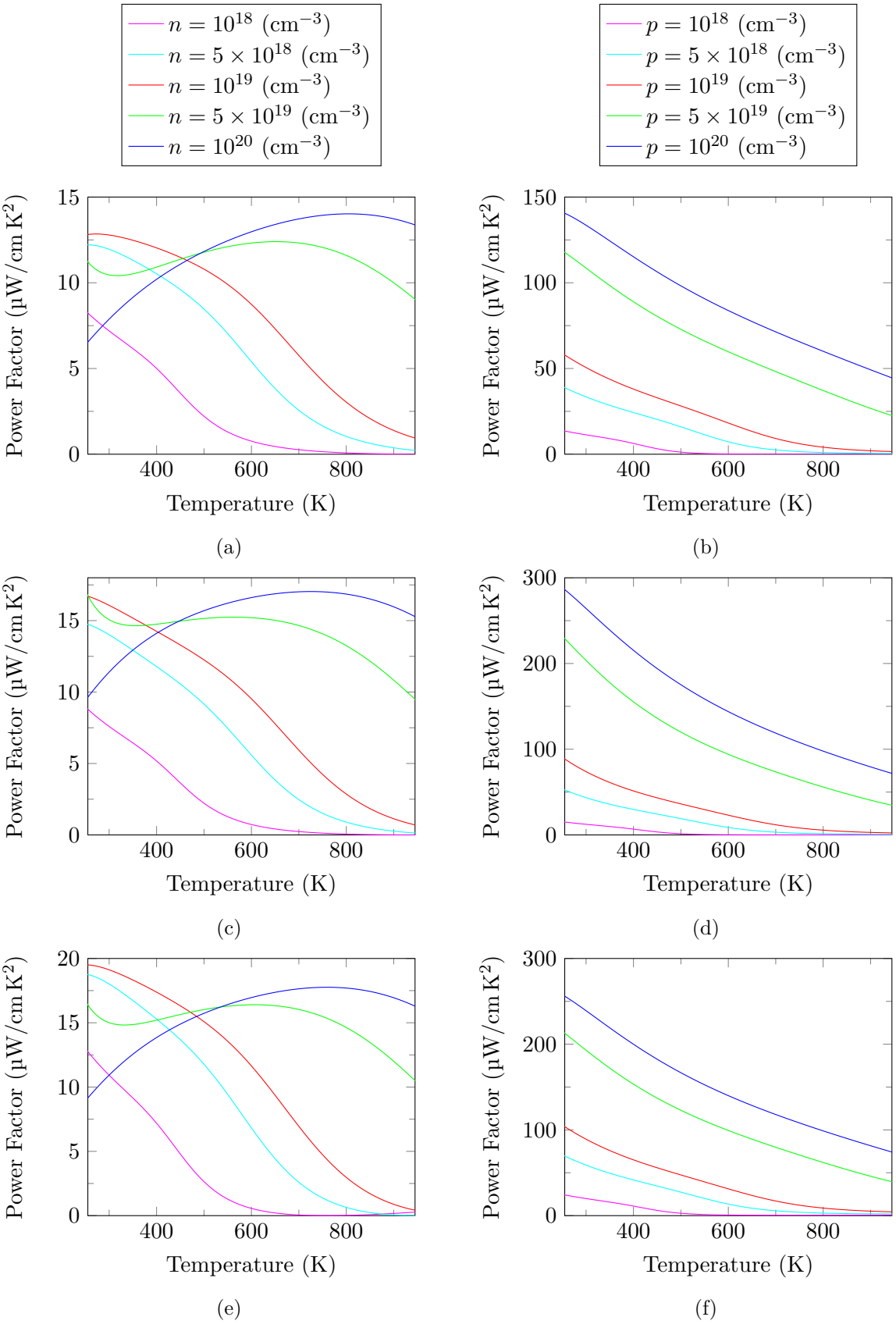

Figure 6.6: Temperature dependence of the Seebeck coefficient at different doping levels computed with a relaxation time taking all phonons scattering mechanisms into account. (a) and (b) : no screening for τ_{po}, (c) and (d) : theoretical screening for τ_{po}, (e) and (f) : fitted model for τ_{po} that includes screening.

6.4 Comparison with Experimental Data

Figure 6.7 shows a comparison between the temperature dependence of the Seebeck coefficient calculated in this work and experimental measurements found in the literature (the articles from which the data are taken are specified in the figure). The calculations were performed with the total relaxation τ_{tot} taking all the scattering mechanisms into account and without screening since we showed that it had no great influence on the estimation of S. A good agreement with experimental data is found for the n-type PbTe except for the low doping level at high temperature that decreases faster in our calculations than what is measured. The Seebeck is however overestimated in case of p-type PbTe, but this can not be due to the relaxation time model since as seen before it happens also for the Seebeck computed with a constant τ.

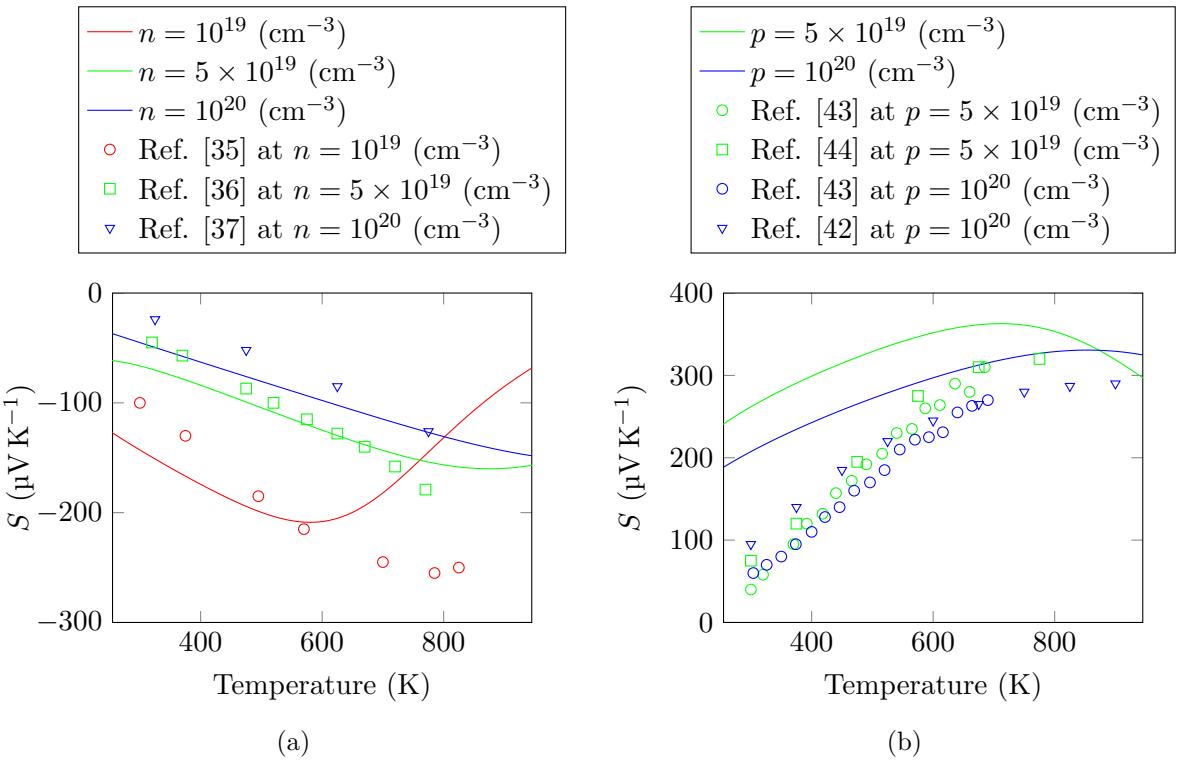

Figure 6.7: Comparison between the Seebeck coefficient at different doping levels computed in this work with the total relaxation time τ_{tot} and the Seebeck coefficient found in the literature from experimental measurements. (a) n-type PbTe, (b) p-type PbTe. The screening is not taken into account since it was shown that it had almost no influence for the estimation of S.

The comparison between the computed electrical conductivity and experimental measurements at different doping levels is presented on Figure 6.8. Again the calculations were realised with the total relaxation time for the three models for screening in τ_{po}. It is found that for both n- and p-type PbTe, the temperature dependence is in good agreement with experimental data. However in case of n-type material, σ is quite underestimated. The inclusion of screening leads to better results but σ is still a little bit lower than what is measured, suggesting that the influence of the scattering may be overestimated. But on the opposite, the conductivity for p-type PbTe is slightly overestimated and this get worse when screening is included. Therefore we can not conclude if the scattering was over- or underestimated and this difference may come from the fact that we used the same effective mass for both electrons and holes. A more specific model for the relaxation time using the *ab-initio* band structure instead of a parabolic band structure would probably give better results.

Finally, the comparison between the power factor calculated in this work and coming from experimental data is presented on the Figure 6.9. One can notice that for n-type PbTe, except

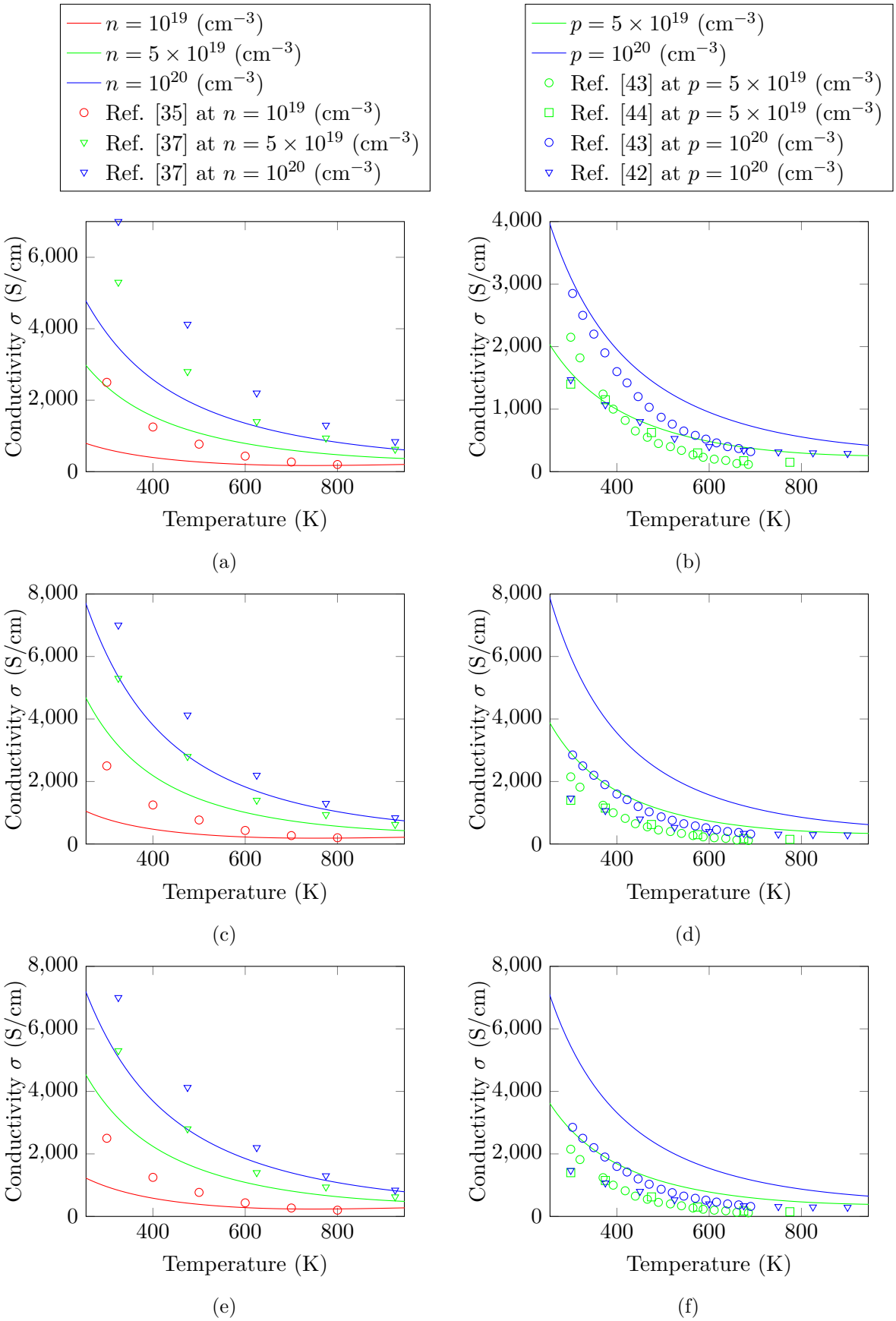

Figure 6.8: Comparison between σ at different doping levels computed in this work with the total relaxation time τ_{tot} and σ found in the literature from experimental measurements. (a) and (b) : no screening for τ_{po}, (c) and (d) : theoretical screening for τ_{po}, (e) and (f) : fitted model for τ_{po} that includes screening.

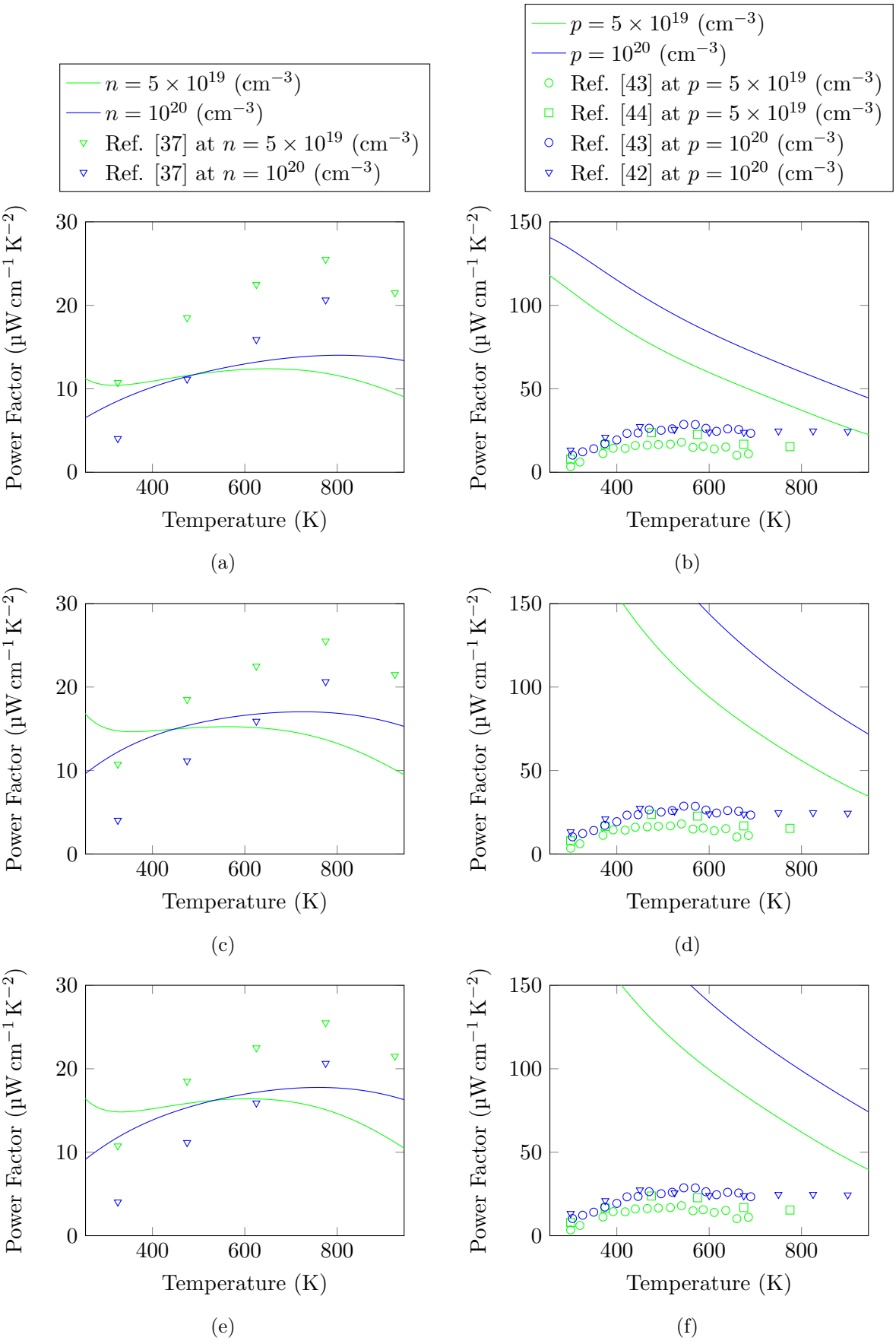

Figure 6.9: Comparison between PF at different doping levels computed in this work with the total relaxation time τ_{tot} and PF found in the literature from experimental measurements. (a) and (b) : no screening for τ_{po}, (c) and (d) : theoretical screening for τ_{po}, (e) and (f) : fitted model for τ_{po} that includes screening.

at low temperature the T-dependence is quite in good agreement with experimental data but that due to the underestimation of the conductivity, the PF is also a little bit smaller than measured. Again the inclusion of screening gives better results since σ is less underestimated in this case. For the p-type material, the overestimation of S and σ leads to a huge overestimation of the power factor in comparison to what is usually found and as expected, the inclusion of screening leads to even worse results.

These quite bad results come from the multiplication of the differences between the computed S and σ and the ones coming from the literature. However it is important to remind that separately, a correct temperature dependence was found with our total energy and temperature dependent relaxation time model, what was really not the case with a constant τ.

Chapter 7

Conclusion

The main objective of the present master thesis was to analyse the influence of the *Relaxation Time Approximation* in the *ab-initio* computation of thermoelectric properties of materials. The lead telluride was chosen as reference material for this study since it is a well known thermoelectric material for which many experimental data can be found in the literature. First in Chapter 2 we remind the basis of the thermoelectric effect and how it can be used to product electricity from heat waste sources. In Chapter 3 the general properties of lead telluride are presented, we also describe the convergence studies as well as the band structure calculation that was subsequently used to compute the transport coefficients. The calculations were performed in the framework of the Boltzmann transport equation that is derived in Chapter 4. In order to check the influence of the RTA, different models for the relaxation time were tested, from a very simple constant τ to energy and temperature-dependent models. In this work we focused on the temperatures between 300 and 900 K, which correspond to the range of temperatures where PbTe exhibits good thermolectric properties. At these temperatures, phonon scattering is the main relaxation mechanism and consequently we chose to include three different types of phonon scattering in this work, namely deformation potential by acoustic and optical phonons and polar optical phonon scattering. For the latter, we also tried models including the screening of the ions Coulomb potential by charge carriers themselves, resulting in reduced influence of this relaxation mechanism. All these models are derived and explained in Chapter 5.

Chapter 6 presents the resulting transport coefficients. The calculations showed that the Seebeck coefficient and its temperature dependence are already correctly estimated with the simple model of a constant τ and that more sophisticated models increase complexity without bringing significant added precision. However, the constant τ model resulted in almost no temperature dependence for the electrical conductivity, which is totally different from experimental data. The implementation of an energy and temperature-dependent τ led to $\sigma(T)$ curves that showed the correct shape but were underestimated in magnitude for n-type PbTe and overestimated for p-type material. The screened models for polar optical scattering gave better results for the n-type PbTe, since the influence of this mechanism was reduced, but worse results for the p-type PbTe. Therefore it is not easy to determine whether this was due to a bad estimation of the magnitude of scattering, through wrong deformation potential constants for example, or to some other reason. One possible cause for this difference between n- and p-type PbTe is that we used the same effective mass for both electrons and holes through the parabolic model for the band structure in the calculation of τ. Finally the calculation of the power factor from the computed S and σ gave results in quite good agreement with experimental data for the n-type material but severely overestimated results for the p-type PbTe.

In conclusion, a correct estimation of S is found even with a constant relaxation time and the implementation of an energy and temperature-dependent model led to the correct trend for the temperature dependence of both S and σ. However some improvements are possible in the estimation of the magnitude of the different scattering mechanisms.

This work could be continued in an interesting way by trying to directly use the *ab-initio* band structure for the calculation of the relaxation time instead of the parabolic model used in this work. In this way, the anisotropy of the material would be directly taken into account as well as the difference of effective mass between holes and electrons. This would require to carefully study the hypothesis made for obtaining the formula of the different τ and also to consequently modify the τ model in the BoltzTraP program, but the results for the electrical conductivity would probably be in better agreement with experimental data. Moreover, some of the parameters used for the calculation of the relaxation time, such as the deformation potentials for example, were taken from the literature but they could also be computed *ab-initio*. Finally, for other materials at other temperatures, different scattering mechanisms such as scattering by ionised impurities or charged vacancies are also present and should be included in the calculation of the total relaxation time.

References

[1] Z. H. Dughaish. Lead telluride as a thermoelectric material for thermoelectric power generation. *Physica B: Condensed Matter*, 322(1):205–223, 2002.

[2] Y. Pei, H. Wang, and G. J. Snyder. Band engineering of thermoelectric materials. *Advanced materials*, 24(46):6125–6135, 2012.

[3] X. Gonze and al. *Abinit.org*. `http://www.abinit.org`, 2015.

[4] G. K. H. Madsen and D. J. Singh. Boltztrap. a code for calculating band-structure dependent quantities. *Computer Physics Communications*, 175(1):67–71, 2006.

[5] Wikipedia. *Thermoelectric materials*. `https://en.wikipedia.org/wiki/Thermoelectric_materials`, 2016.

[6] Wikipedia. *Thermoelectric effect*. `https://en.wikipedia.org/wiki/Thermoelectric_effect`, 2016.

[7] Wikipedia. *Thermoelectric generator*. `https://en.wikipedia.org/wiki/Thermoelectric_generator`, 2016.

[8] M. W. Wu, N. J. M. Horing, and H. L. Cui. Phonon-drag effects on thermoelectric power. *Physical Review B*, 54(8):5438, 1996.

[9] Woodbank Communications Ltd. *Direct Conversion of Heat Energy to Electrical Energy: Thermocouple Electric Generators*. `http://www.mpoweruk.com/thermoelectricity.htm`, 2005.

[10] M. Wagner. *Simulation of Thermoelectric Devices: Characterization of Materials*. `http://www.iue.tuwien.ac.at/phd/mwagner/node49.html`, 2016.

[11] M. Jonson and G. D. Mahan. Mott's formula for the thermopower and the wiedemann-franz law. *Physical Review B*, 21(10):4223, 1980.

[12] D. I. Bilc, G. Hautier, D. Waroquiers, G. M. Rignanese, and P. Ghosez. Low-dimensional transport and large thermoelectric power factors in bulk semiconductors by band engineering of highly directional electronic states. *Physical review letters*, 114(13):136601, 2015.

[13] G. J. Snyder and E. S. Toberer. Complex thermoelectric materials. *Nature materials*, 7(2):105–114, 2008.

[14] UC Davis ChemWiki. *Structures of Simple Binary Compounds*. `http://chemwiki.ucdavis.edu/?title=Textbook_Maps/General_Chemistry_Textbook_Maps/Map:_Chemistry_(Averill_%26_Eldredge)/12:_Solids/12.3:_Structures_of_Simple_Binary_Compounds`, 2016.

[15] K. Momma and F. Izumi. Vesta 3 for three-dimensional visualization of crystal, volumetric and morphology data. *Journal of Applied Crystallography*, 44(6):1272–1276, 2011.

[16] Freie Universität Berlin. *Chapter 8: Spin-orbit interaction.* http://www.diss.fu-berlin.de/diss/servlets/MCRFileNodeServlet/FUDISS_derivate_000000003802/10_chapter8.pdf?hosts=, 2016.

[17] Wikipedia. *Spin-orbit interaction.* https://en.wikipedia.org/wiki/Spin%E2%80%93orbit_interaction, 2016.

[18] C. Hartwigsen, S. Gœdecker, and J. Hutter. Relativistic separable dual-space gaussian pseudopotentials from h to rn. *Physical Review B*, 58(7):3641, 1998.

[19] H. J. Monkhorst and J. D. Pack. Special points for brillouin-zone integrations. *Physical review B*, 13(12):5188, 1976.

[20] Wikipedia. *Broyden–Fletcher–Goldfarb–Shanno algorithm.* https://en.wikipedia.org/wiki/Broyden%E2%80%93Fletcher%E2%80%93Goldfarb%E2%80%93Shanno_algorithm, 2016.

[21] Materials Project. *Lead Telluride.* https://www.materialsproject.org/materials/mp-19717/.

[22] P. E. Blöchl. Projector augmented-wave method. *Physical Review B*, 50(24):17953, 1994.

[23] J. P. Perdew, K. Burke, and M. Ernzerhof. Generalized gradient approximation made simple. *Physical review letters*, 77(18):3865, 1996.

[24] W. Setyawan and S. Curtarolo. High-throughput electronic band structure calculations: Challenges and tools. *Computational Materials Science*, 49(2):299–312, 2010.

[25] Y. W. Tsang and M. L. Cohen. Calculation of the temperature dependence of the energy gaps in pbte and snte. *Physical Review B*, 3(4):1254, 1971.

[26] J. P. Perdew. Density functional theory and the band gap problem. *International Journal of Quantum Chemistry*, 28(S19):497–523, 1985.

[27] B. M. Askerov. *Electron transport phenomena in semiconductors*, volume 394. World Scientific, 1994.

[28] M. Lundstrom. *Fundamentals of carrier transport.* Cambridge University Press, 2009.

[29] L. A. Righi. Chapter 1 boltzmann tranport. http://coral.ufsm.br/righi/Materiais/FIGS/CH01.pdf. Universidade Federal de Santa Maria.

[30] S. Ahmad and S. D. Mahanti. Energy and temperature dependence of relaxation time and wiedemann-franz law on pbte. *Physical Review B*, 81(16):165203, 2010.

[31] Wikipedia. *Phonon.* https://en.wikipedia.org/wiki/Phonon, 2016.

[32] J. Bardeen and W. Shockley. Deformation potentials and mobilities in non-polar crystals. *Physical Review*, 80(1):72, 1950.

[33] H. Ehrenreich. Screening effects in polar semiconductors. *Journal of Physics and Chemistry of Solids*, 8:130–135, 1959.

[34] D. M. Zayachuk. The dominant mechanisms of charge-carrier scattering in lead telluride. *Semiconductors*, 31(2):173–176, 1997.

[35] G. W. Johnson. The seebeck coefficient and electrical resistivity of n-type pbte between 20° c and 550° c†. *INTERNATIONAL JOURNAL OF ELECTRONICS*, 16(5):497–507, 1964.

[36] Y. I. Ravich, B. A. Efimova, and V. I. Tamarchenko. Scattering of current carriers and transport phenomena in lead chalcogenides. *physica status solidi (b)*, 43(1):11–33, 1971.

[37] D. I. Bilc, S. D. Mahanti, and M. G. Kanatzidis. Electronic transport properties of pbte and agpb m sbte 2+ m systems. *Physical Review B*, 74(12):125202, 2006.

[38] Wikipedia. *Density Functional Theory.* `http://en.wikipedia.org/wiki/Density_functional_theory`, 2015.

[39] O. Madelung, U. Rössler, and M. Schulz, editors. *Non-Tetrahedrally Bonded Elements and Binary Compounds I*, chapter Lead telluride (PbTe) crystal structure, lattice parameters, thermal expansion, pages 1–3. Springer Berlin Heidelberg, Berlin, Heidelberg, 1998.

[40] T. J. Scheidemantel, C. Ambrosch-Draxl, T. Thonhauser, J. V. Badding, and J. O. Sofo. Transport coefficients from first-principles calculations. *Physical Review B*, 68(12):125210, 2003.

[41] Y. I. Ravich, B. A. Efimova, and V. I. Tamarchenko. Scattering of current carriers and transport phenomena in lead chalcogenides. *physica status solidi (b)*, 43(1):11–33, 1971.

[42] L. D. Zhao, H. J. Wu, S. Q. Hao, C. I. Wu, X. Y. Zhou, K. Biswas, J. Q. He, T. P. Hogan, C. Uher, C. Wolverton, et al. All-scale hierarchical thermoelectrics: Mgte in pbte facilitates valence band convergence and suppresses bipolar thermal transport for high performance. *Energy & Environmental Science*, 6(11):3346–3355, 2013.

[43] I. Androulakis, I. Todorov, D. Y. Chung, S. Ballikaya, G. Wang, C. Uher, and M. Kanatzidis. High thermoelectric efficiency in co-doped degenerate p-type pbte. In *MRS Proceedings*, volume 1267, pages 1267–DD04. Cambridge Univ Press, 2010.

[44] Q. Zhang, F. Cao, W. Liu, K. Lukas, B. Yu, S. Chen, C. Opeil, D. Broido, G. Chen, and Z. Ren. Heavy doping and band engineering by potassium to improve the thermoelectric figure of merit in p-type pbte, pbse, and pbte1–y se y. *Journal of the American chemical society*, 134(24):10031–10038, 2012.

[45] X. Gonze, Charlier J. C., and G. M. Rignanese. *MAPR 2451 - Atomistic and nanoscopic simulations*, 2015.

[46] L. Piraux. *MAPR 2471 - Phénomènes de transport dans les solides et les nanostructures*, 2015.

Rue Archimède, 1 bte L6.11.01, 1348 Louvain-la-Neuve **www.uclouvain.be/epl**